THE EFFECT OF TIP CLEARANCE FLOWS
ON PERFORMANCE OF AXIAL FLOW COMPRESSORS

Thesis by

Allen Dean Williams

Lieutenant, United States Navy

In Partial Fulfillment of the Requirements

For the Degree of

Aeronautical Engineer

California Institute of Technology

Pasadena, California

1960

ACKNOWLEDGEMENTS

The author wishes to express his sincere thanks to Drs. W. D. Rannie and A. J. Acosta for their helpful guidance and suggestions during the course of this research.

Many members of the Hydrodynamics Laboratory Staff aided in various ways; in particular, J. Kingan and C. Eastvedt.

The efforts of Mrs. Joan McFarland, Mrs. Roberta Duffy, and Mrs. Betty Wood made possible the report in final form.

ABSTRACT

The change in rotor performance with tip clearance of an axial flow compressor over a wide range of flow rates above stall was investigated to gain more understanding of the effect of the tip flow mechanism on rotor performance.

The experimental results were compared with a flow model proposed previously and found to be in reasonable agreement.

TABLE OF CONTENTS

SUMMARY

The effect of tip clearance flows on the efficiency of compressors has been the subject of several investigations in the past. In general, however, the loss mechanism has not been well understood.

Rains investigated the tip clearance flow using flow visualization, and proposed a perfect fluid model with corrections for real fluid effects to describe quantitatively the loss mechanism, and compared his model with experimental results at the design flow rate. The model proposed was analogous to flow through a narrow slot in a wing of finite chord. Flow visualization showed that the vortex sheet formed by the tip clearance flow entering the free stream flow rolled up into a single vortex. Thus, it was assumed that the flux of kinetic energy associated with the flow normal to the blade created the rolled up vortex and was not recovered. To handle the real fluid effects the main contribution was taken to be the "scraping up" of the case boundary layer, whereby the pressure difference across the blade tip was increased, thus increasing the losses. Rains approximated this by a simplified analysis of shear flow in a corner.

The purpose of this investigation was to gain more understanding of the tip flow mechanism by determining the change in rotor performance with tip clearance over a wide range of flow rates and comparing these results with the model described above. Detailed surveys of static pressure, flow direction, and total pressure were made ahead and behind the rotor to obtain integrated averages of pressure, flow rate and work input.

It was found that the reduction in work coefficient with tip clearance was less than that predicted by the model above. It was felt that if the scraping flow were analyzed in a more realistic fashion, the agreement might be better.

In the case of reduction in total pressure coefficient and efficiency it was found that by including the scraping flow the changes were overestimated. Neglecting the scraping flow, the reduction in efficiency due to tip clearance was overestimated near stall and underestimated at the high flow rate above design. Due to the scattering of experimental results and the small changes involved, i. e., most changes were not much more than the order of accuracy of the experiments, it was felt that one could only discuss trends in evaluating the validity of the proposed model. In this respect, it was felt that the model was a valid one, since the order of magnitude of the losses was in reasonable agreement with experimental results over a wide range of flow rates, and variations in calculated and experimental efficiency drop with flow rate showed similar trends.

The agreement between theory and experiment was not as close as that found by Rains. However, the tests reported here covered a much larger range than those of Rains, and their internal consistency indicates that they are as reliable as the previous experiments.

I. INTRODUCTION

For good efficiency of a gas turbine cycle, it is axiomatic that the compressor have a high efficiency. Among the losses suffered by the compressor are those due to leakage flows through the tip clearance. It has been shown(1, 2, 3) that the variation of tip clearance has an important effect on pump and compressor performance. In particular, Rains(2) investigated in detail the tip clearance flow mechanism and variation in compressor performance with tip clearance at the design flow rate. He introduced a perfect fluid flow model and corrections for real fluid effects to compare with experiments, so that variation in compressor performance could be estimated for other operating conditions and other machines.

The present investigation is concerned with determining the effect of tip clearance on compressor performance, not only at design conditions, but also through a range of flow rates from near stall to well above design, for the purpose of gaining more understanding of the tip flow mechanism and to extend the range of comparison of the experiments with the perfect fluid model and real fluid corrections given in Reference 2.

II. EQUIPMENT AND EXPERIMENTAL TECHNIQUES

A. Pump and Pump Circuit

The turbomachine and tunnel system used for this investigation consisted of a closed circuit tunnel, Figure 1, containing an axial flow pump, Figure 2, which served both as a pumping unit for the tunnel and test section for the experiment. The system is described in detail in References 2 and 4. The turbomachine was a scaled version of the axial flow air compressor discussed in Reference 5. Thus, although the working fluid was water, the turbomachine corresponded to an axial flow air compressor operating at a Reynolds number of order 100,000 based on mean axial velocity and blade chord, rather than to a conventional axial flow pump.

The test unit was approximately forty inches long, with a fourteen inch inside diameter and could accommodate up to three stages of blading. For this investigation, only one stage was used in a spread configuration to facilitate isolation of rotor characteristics. The entrance vanes were located (as indicated in Figure 2) ahead of Station 2; the first stage, consisting of a rotor row and stator row were left out, and the rotor was placed between Stations 4 and 5. The stator was also displaced one stage behind the rotor and located between Stations 7 and 8, followed by two rows of straightening vanes. A lucite viewing window was located in the test section that extended the length of the rotor.

The machine was driven by a dynamometer mounted vertically about three feet above the circuit as shown in Figure 1. The power was supplied by a 30 KW thyratron rectifier unit.

B. Blade Design

The blading was designed to produce a free vortex flow at an average flow coefficient $\bar{\phi} = 0.45$, an average work coefficient $\bar{\Psi} = 0.40$, and a symmetrical velocity diagram at $\xi = 0.70$. Detailed surveys showed that the design work coefficient was obtained at an average flow coefficient of 0.42, which was in close agreement with $\bar{\phi} = 0.41$ obtained from previous experiments$^{(2)}$. The differences from design were attributed to the hub and casing boundary layers reducing the effective cross-sectional area of the machine and increasing the mainstream flow rate.

The influence of tip clearance on rotor performance was evaluated in this investigation, and thus the rotor blade characteristics were of primary interest. There were sixteen rotor blades per row with constant chord (1.90 inches) and a parabolic camber line. Details of the blading are given in References 2, 4, and 5. Some essential characteristics are reproduced below:

Radius Ratio	ξ	0.60	0.70	0.80	0.90	1.00
Solidity	c/s	1.15	0.985	0.860	0.765	0.690
Stagger Angle	β^*	15.2°	32.1°	43.8°	51.7°	57.4°
Camber Angle		46.7°	31.0°	20.3°	13.8°	9.8°
Maximum Thickness Ratio		0.12	0.11	0.10	0.09	0.08

C. Instrumentation

A water differential manometer which measured the pressure drop across the contraction nozzle upstream of the test section was used to determine the flow rate.

Detailed flow measurements were made through surveying ports at Stations 2 through 8 as indicated in Figure 2. A plug assembly could be positioned in slots located behind each stationary blade row, Stations 2, 4, 6, and 8, which permitted circumferential surveys over approximately two blade passages in 2 degree increments. A single surveying port was located behind each rotor row at Stations 3, 5, and 7. The probes shown in Figure 3 were used in detailed surveys and were, from left to right, total pressure, yaw, and static pressure. The probe holder permitted radial positioning to 0.01 inches and angular orientations to within 0.1 degrees. Calibration of the yaw and static probes was made in an air jet. The static probe error was found to be 0.3% of dynamic head, in excess of the static pressure. The yaw probe sensitivity was approximately 0.25 degrees, and this was also checked in the Free Surface Water Tunnel in the Hydrodynamics Laboratory. Pressure lines were 1/4-inch Polyflow tubing connected through O-ring push-pull valves to a Statham liquid differential pressure gauge (1 psi full-scale range). Pressure measurements were made using the Statham gauge in conjunction with a Baldwin-Southwark strain gauge bridge. The Statham and strain gauge combination was calibrated frequently using a water differential manometer. A null indication from the above pressure instruments was used in conjunction with the yaw probe to obtain measurements of flow direction. By use of the O-ring valve system, a small and equal head of water could be applied to both sides of the Statham gauge without shutting down the turbomachine, thereby checking for drift in the gauge zero. Static pressure holes were located on the rear side of the case at Stations 1 through 8 and 12.

Rotor blade tip clearance was checked using a depth micrometer through a face plate that was mounted in the flow visualization opening with the lucite window removed.

A differential gear box was used to indicate rotative speeds in unit rpm increments above 100 rpm, while a field rheostat connected to the thyratron rectified unit was used to control the speed. An extension to the rheostat fine control was added, as seen in Figure 4, so that accurate speed control could be maintained by the same person taking pressure readings.

Control of the flow rate was accomplished by use of the hand-operated throttle valve shown in Figure 1.

A torque arm and pan weight system, in which the signal from an electrical displacement pickup was used as a null indicator, was used to measure torque reaction. The mechanical shaft seal downstream of the turbomachine at the elbow was removed to reduce the torque tare. Torque sensitivity was approximately 1% of measured values.

D. Experimental Methods

The flow rate for each test was set using the water differential manometer and throttle valve previously described. The nozzle discharge coefficient, $C_D = 0.988$, was taken from calibrations given in Reference 6, extrapolated to the pipe Reynolds number range, $R_P = 300,000$, of these investigations.

Since the static and total head probes were sensitive to angle for accurate readings, the detailed angle surveys were taken first at each tip clearance. These were then used to position the total and static head probes in the direction of the flow. Thirty-eight radial positions were surveyed over the 2.8 inch annulus, every 0.03 inches in the hub and casing boundary layers, and every 0.10 inches in the mainstream flow. In order to give the inlet guide vane wakes as much time to diffuse as possible, the flow entering the rotor was surveyed at Station 4, just ahead of the rotor. The flow immediately behind the rotor near the tip was very unsteady and hard to measure with the instrumentation used in these tests. For this reason, the surveys behind the rotor were taken at Station 6, one blade row downstream of the rotor exit.

The rpm used for tests at the first tip clearance was 225. Investigations of the blades after completion of these runs indicated a possibility of a small amount of blade bending at the root. To preclude any further bending, the rpm was lowered to 200, reducing the blade loading.

The tip clearance was varied by machining the tips to the desired blade length. To accomplish this, the blades were mounted on a jig of the same diameter as the rotor and machined on a rotary lathe.

E. Test Program

The purpose of the tests was to determine the effect of tip clearance on performance at off-design conditions, hence extending the investigation of Reference 2 where the tests were made only at design point. To accomplish this, average flow rates of $\bar{\phi} = 0.343$, 0.40, 0.45, 0.50, and 0.55 were selected for investigation. The stall region was not investigated because of difficulty in interpretation of detailed measurements. Tip clearances were selected to bracket the range normally used in turbomachinery. Thus, performance was evaluated at each of the above flow rates for $\lambda = 0.0025$, 0.0064, 0.0129, and 0.0254.

Since there were variations from root to tip in flow angle, total pressure and static pressure, especially at off-design flow rates, it was necessary to use detailed surveys of these quantities to determine accurately the change in performance of the turbomachine with changes in flow rate and tip clearance.

Surveys ahead of the rotor were made only at the smallest tip clearance, $\lambda = 0.0025$, and it was assumed that these surveys would not be appreciably affected by variation of tip clearance. Four circumferential stations ahead of the rotor were surveyed at the design flow rate and averaged to properly weight the wake effect of flow leaving the inlet guide vanes. For off-design flow rates, a circumferential station out of the strong wake was selected, and a correction factor applied to integrated values to account for the difference from the circumferential average.

Behind the rotor, only one station circumferentially was surveyed, since it was assumed wakes would be smoothed out while going through the rotor.

III. RESULTS

A. Estimation of Inlet Guide Vane Losses

Losses through the inlet guide vanes should vary as the square of the flow rate(7). As seen in Figure 5, the off-design values are too high, according to the above criteria, using the design flow rate value as a basis. Though the circumferential station selected for off-design surveys was not in a strong wake at the design flow rate, it is felt that wakes could have shifted with change in flow rate giving higher losses than the circumferential average. Therefore, those detailed surveys taken at the design flow rate are averaged circumferentially and assumed to vary as the square of the average flow coefficient.

B. Rotor Performance - Averaged Results

The average flow coefficient is determined by numerical integration,

$$\bar{\phi} = \frac{\text{mean axial velocity}}{\text{tip speed}} = \frac{\int_{\xi_i}^{\xi_o} \phi \xi \, d\xi}{\int_{\xi_i}^{\xi_o} \xi \, d\xi} .$$

The average pressure coefficient is determined similarly,

$$\bar{\psi} = \frac{P_{t2} - P_{t1}}{\frac{1}{2}\rho u_o^2} = \frac{\int_{\xi_i}^{\xi_o} \phi \xi \, \psi d\xi}{\int_{\xi_i}^{\xi_o} \phi \xi \, d\xi} .$$

The variation of average pressure coefficient with average flow coefficient, Figure 6, is seen to be almost linear, where $\bar{\psi}$ increases with decreasing flow rates from $\bar{\phi} = .55$ to slightly below design. The variation becomes increasingly non-linear as the stall flow rate is approached.

A similar change in $\bar{\psi}$ with flow coefficient is seen at all tip clearances investigated.

The variation in average work coefficient, $\bar{\Psi}$, with average flow coefficient, Figure 7, is similar to that of $\bar{\psi}$ with $\bar{\phi}$; however, the variation is more nearly linear as would be expected.

The variation of average pressure coefficient with tip clearance at the various flow rates, as shown in Figure 8, is seen to be erratic. Values plotted in Figure 6 have been referred to common flow rates before being cross-plotted in Figure 8. Though erratic, the results show that the pressure coefficient drops nearly linearly with increasing tip clearance at each flow rate. The drop in average pressure coefficient with tip clearance is seen to be greatest at the lowest flow rate and decreases with increasing flow rate.

$\bar{\phi}$	$\Delta\bar{\psi}_{\lambda = 0 \text{ to } \lambda = 0.0254}$
0.343	0.025
0.40	0.025
0.45	0.020
0.50	0.015
0.55	0.010

The average work coefficient is determined from rotor torque measurements, $\bar{\Psi} = T/\frac{1}{2}\rho u_o^2 R_o A\bar{\phi}$. As seen in Figure 9, the average work coefficient is nearly constant with changes in tip clearance over the range investigated. Results are similar at all flow rates. The slight change shows a trend of decreasing work coefficient with tip clearance, $\Delta\bar{\Psi} \cong 0.005$, from $\lambda = 0$ to $\lambda = 0.0254$.

The efficiency of the rotor is defined as the ratio of the average total pressure rise through the rotor to average work input by the rotor, $E = \bar{\psi}/\bar{\Psi}$. Values of average pressure coefficient and average work coefficient used in determining the rotor efficiency were taken from the faired curves of Figures 8 and 9. As seen in Figure 10, the efficiency increases with decreasing flow rate until stall is approached, where the efficiency falls off. The maximum efficiency occurs at a flow rate below design, $\bar{\phi} = 0.40$, approximately. It appears, referring to Figure 10, that the efficiency values at $\bar{\phi} = 0.40$ and $\bar{\phi} = 0.50$ are consistently high. Since only one circumferential station was surveyed behind the rotor, there is a possibility that guide vane wakes were carried through the rotor. Though they would be much smaller than wakes ahead of the rotor, they would tend to change circumferential position with flow rate. Since a small change in the pressure coefficient will make a large change in efficiency, it is felt that the wakes could account for some of the erratic behavior of pressure coefficient and efficiency.

The efficiency clearly decreases with tip clearance, as seen in Figure 11. The change is largest at the lowest flow rate, and decreases with increasing flow rate.

$\bar{\phi}$	$\Delta E_{\lambda = 0 \text{ to } \lambda = 0.0254}$
0.343	.047
0.40	.047
0.45	.046
0.50	.040
0.55	.037

C. Rotor Performance - Detailed Surveys

1. *Variation with flow rate.* Excluding the boundary layer effect, it is seen from Figures 12, 13, 14, and 15 that the axial velocity behind the rotor decreases from the blade root to the tip at the flow rates above design. The slope flattens as the flow rate decreases and is approximately

zero at the design flow rate, which would be expected from free vortex blading(5). As the average flow rate is further decreased, the axial velocity increases toward the tip. At the flow rate near stall, $\bar{\phi} = .343$, the axial velocity in the tip region drops off earlier than at the higher flow rates. It is felt that this could be caused by tip stalling. The above tip distribution affects the overall radial distribution by increasing the axial velocity near the hub. The axial velocity entering the rotor is seen from Figure 16 to be nearly constant at the design flow rate outside the boundary layer. It was assumed that this distribution remained constant with flow rate.

The total head or pressure coefficient, ψ, across the rotor is a measure of the total pressure added to the flow by the rotor. It is seen from Figures 17, 18, 19, and 20 that the portion of the blade near the hub is highly loaded at flow rates above design, while the tip loading is low. As the flow rate is lowered, the loading becomes more nearly constant with only small changes in loading below the design flow rate. As seen in the surveys of axial velocity, Figure 12, and total head coefficient, Figure 17, the local wakes shift radially with change in flow rate.

The work coefficient is a measure of work input by the rotor through a change in the whirl component of velocity. At flow rates below design, the tip is very highly loaded (Figures 17, 18, 19 and 20). As the flow rate increases, the tip loading decreases and the loading near the root of the blades increases.

2. Variation with tip clearance. The axial velocity distribution is seen to remain almost constant with increasing tip clearance at the design flow rate and higher, Figures 21 and 21a. At the two flow rates below

design, $\bar{\phi} = .343$ and $\bar{\phi} = .40$, the axial velocity at the tip drops off rapidly at the largest tip clearance investigated, $\lambda = 0.0254$. This drop could be attributed to tip stall. Measurements of flow angle and total pressure in tip region at $\lambda = 0.0254$ were very erratic, indicating a very unsteady flow or stalled condition.

As seen in Figures 22 and 22a, there is very little change in radial distribution of total pressure rise through the rotor with change in tip clearance except in the tip region. At the design flow rate and above, the pressure rise in the tip region clearly drops off with increasing tip clearance. Near stall, $\bar{\phi} = .343$, there is a slight increase in tip loading with increasing tip clearance. This may possibly be explained by the increased tip clearance relieving a flow blockage near the tip. It is clear from Figures 21 and 22 that the wakes remain in the same radial position and are of the same magnitude with changing tip clearance at a given flow rate.

Comparison of Figures 17, 18, 19, and 20 shows an erratic variation of work coefficient with tip clearance. These readings would be expected to be less accurate since the change in the whirl component of velocity is not large. Thus, a small error in one of the whirl components would give a large error in the change of whirl. Generally, the work coefficient in the tip region does drop off with increasing tip clearance at the design flow rate and above.

IV. TIP CLEARANCE FLOW MODEL AND COMPARISON WITHRESULTS

A. Introduction.

The flow of a perfect fluid through a tip clearance can be thought of as a flow through a slotted wing with the wall representing the plane of symmetry through the slot. Flow through a slotted wing has been analyzed using lifting line theory; however, the assumptions required for this type of treatment are that the vortices be shed at the trailing edge of the wing as the circulation drops to zero at the tip and that the slot be large compared with the wing chord.

A more reasonable model of the flow through a narrow slot is one in which the vortices are shed along the edges of the slot rather than at the trailing edge. Flow visualization experiments by Rains(2) have shown that the above model, where the Kutta condition is satisfied along the chord at the blade tip, is a valid model of the flow considered. The problem that immediately follows is how to apply this model to a turbomachine to determine the effect of tip clearance on efficiency and work input to the flow, and what corrections should be made to account for real fluid effects.

The flow in the tip clearance can be thought of as having uniform velocity in the direction of the chord, which is carried through from the pressure to suction side essentially unchanged for blades of small thickness. The velocity perpendicular to the chord is

$$u_n = \frac{2(p_1 - p_2)^{\frac{1}{2}}}{\rho} ,$$

where p_1 and p_2 are static pressures on the pressure and suction side of the blade away from the tip, and in general, u_n varies along the chord.

As shown by Rains(2), the most important real fluid effect is the "scraping up" of the case boundary layer by the rotating blades. In a compressor, this action tends to increase the pressure on the pressure side of the blade, thus increasing both the pressure drop across the blade and the flow through the tip clearance.

B. Reduction of Work Input

The factors that cause a reduction of work input by the rotor due to tip clearance are: (1) physically there can be no work done by the blades on flow through the clearance; (2) the pressure drop across the blade serves to increase the flow through the clearance, thus reducing the available fluid on which the blade can do work.

The work done by the rotor may be expressed as

$$(1)\quad W = \int_A \Delta c_u \rho c_a \, dA \quad ,$$

which may be expressed as

$$(2)\quad W = \tfrac{1}{2} \rho u_o^2 R_o 2\pi \bar{\phi} \bar{\Psi} \int_{R_i}^{R_o - \delta} dr$$

where $\bar{\Psi}$ is the average work coefficient and $\Psi = \frac{2\Delta c_u}{u} \frac{r}{R_o}$. Then the reduction in work due to the physical reduction of blade working area is:

$$(3)\quad \frac{\Delta \bar{\Psi}}{\bar{\Psi}} = \frac{\phi_o \Psi_o}{\bar{\phi} \bar{\Psi}} \frac{\delta}{b} \quad .$$

The reduction of work input given by the pressure difference across the blade can be determined by evaluation of the flow into a sharp-edged orifice. This flow can be solved using the hodograph method[(8)], where pressure on the pressure side of the blade is taken as stagnation pressure and varies as the tip is approached while the pressure distribution on the suction side of the blade is essentially unaffected by the tip flow. With reference to Figure 23, it can be shown that along $y = 0$,

$$(4)\quad \frac{x}{\delta} = \frac{2}{\pi + 2}\left[\sin^{-1}\left(\frac{2V}{1 + V^2}\right) + \frac{1}{V}\right]$$

where $V = -\frac{u}{U}$. The integrated pressure deficiency, $\int_{\delta}^{\infty} (p_o - p)\,dx$ can then be found in terms of δ to be:

$$\frac{\pi - 2}{\pi + 2}\,\delta\left[\tfrac{1}{2}\rho U^2\right] = \tfrac{1}{2}\rho U^2 \delta' ,$$

where δ' represents an increase in tip clearance to account for the pressure deficiency. Then the effective tip clearance is seen to be

$$(5)\quad \delta + \delta' = \frac{2\pi}{\pi + 2}\,\delta ,$$

and the work reduction is

$$(6)\quad \frac{\Delta\bar{\Psi}}{\bar{\Psi}} = \frac{2\pi}{\pi + 2}\,\frac{\phi_o \Psi_o}{\bar{\phi}\,\bar{\Psi}}\,\frac{\delta}{b} .$$

If the flow separates and reattaches before leaving the clearance, pressure recovery is obtained and the resulting reduction is that given by Equation 3.

To estimate the effect of "scraping up" the boundary layer, Rains[(2)] introduces a mathematical model where a uniform distribution of vorticity was assumed in order to compute approximately the boundary layer flow into a corner. His result gives the pressure distribution along the y axis as

$$(7)\quad \frac{p - p_1}{\frac{1}{2}\rho u_o^2 \cos^2 \beta_o^*} = 1 - \left[(y/\delta^*) - \frac{1}{4}(y/\delta^*)^2 \right]^2 = I(y/\delta^*) \quad ,$$

where δ^* is the displacement thickness of the boundary layer. Integration of Equation 7 gives the force increase on the blade,

$$(8)\quad \int_o^{c_o} \int_{\delta_t}^{2\delta^*} (p-p_1)\,dx\,dy = c_o \delta^* \rho \frac{u_o^2}{2} \cos^2 \beta_o^* \times \left[\frac{14}{15} - \left(\frac{\delta}{\delta^*}\right) + \frac{1}{3}\left(\frac{\delta}{\delta^*}\right)^3 - \frac{1}{8}\left(\frac{\delta}{\delta^*}\right)^4 + \frac{1}{80}\left(\frac{\delta}{\delta^*}\right)^5 \right] \quad ,$$

and the reduction of work input with tip clearance is

$$(9)\quad \frac{\Delta \overline{\Psi}}{\overline{\Psi}} = 2 \frac{c_o}{\delta} \frac{\delta^*}{R_o} \frac{\cos^3 B_o^*}{(1-\xi_i^2)} \frac{1}{\phi \overline{\Psi}} \left[- \left(\frac{\delta}{\delta^*}\right) + \frac{1}{3}\left(\frac{\delta}{\delta^*}\right)^3 - \frac{1}{8}\left(\frac{\delta}{\delta^*}\right)^4 + \frac{1}{80}\left(\frac{\delta}{\delta^*}\right)^5 \right] .$$

It is seen from Equation 9 that the scraping flow approximation breaks down when the tip clearance gets appreciably larger than the displacement thickness. In fact, when compared with experimental results in Figure 9 and Table I, it appears that the scraping flow effect with tip clearance should be completely discarded. The difference in change of work coefficient with tip clearance as computed from Equation 3 and that observed in the experiment is of the order of 1% of the average work coefficient. This difference is of the same order as the accuracy of the torque measurements, from which the experimental work coefficient was derived. Thus, it is felt that more accurate torque measurements would be required to evaluate the work reduction mechanism. When the order of magnitude of the reduction of work input is known, it can be compensated for by designing for increased work input by the blades.

C. Efficiency Drop

In order to compute the decrease in efficiency due to tip clearance, a loss mechanism was assumed, whereby the flux of kinetic energy associated with the flow normal to the blade was taken as the total power loss. Flow visualization experiments by Rains(2) have shown that the vortex sheet formed by the tip clearance flow entering the free stream flow rolls up into a single vortex. By the same method he has shown the importance of pressure difference across the blade on flow through the tip clearance, i.e., as the pump flow rate increases, the pressure difference across the blade decreases and less flow goes through the clearance. The above loss assumption implies that the flux of kinetic energy associated with the flow normal to the blade creates the rolled-up vortex and is not recovered.

The power loss on one blade row is given by

$$(10)\quad N\int_o^c \tfrac{1}{2}\rho u_n^2 u_n \delta\, dx = N u_o^3 \frac{\rho}{2} \delta\, c_o \int_o^1 \left(\frac{u_n}{u_o}\right)^3 d\left(\frac{x}{c_o}\right) ,$$

where N is the number of blades. This can be written as

$$(11)\quad \text{Power loss} = N u_o^3 \frac{\rho}{2} \delta\, c_o K \left(\frac{\Delta p}{\tfrac{1}{2}\rho u_o^2}\right)^{3/2} ,$$

if the Bernoulli equation $\Delta p = \tfrac{1}{2}\rho u_n^2$ is used, and K is a factor to account for a chordwise pressure loading of the blade that is other than constant.

With reference to Figure 24, it can be seen that the change in angular momentum can be written as:

(12) $(c_{u_2} - c_{u_1}) \rho \, c_a = \frac{L}{s} \cos \beta_\infty - \frac{D}{s} \sin \beta_\infty$

neglecting three-dimensional effects, and the change in momentum in the axial direction can be expressed as

(13) $p_2 - p_1 = \frac{L}{s} \sin \beta_\infty - \frac{D}{s} \cos \beta_\infty$.

Multiplying Equation 12 by $\cos \beta_\infty$ and Equation 13 by $\sin \beta_\infty$, then adding the two equations, the lift may be expressed as

(14) $\frac{L}{s} = (w_{u_1} - w_{u_2}) \rho \, c_a \cos \beta_\infty + (p_2 - p_1) \sin \beta_\infty$.

The change in total pressure through the rotor can be expressed in terms of the change in angular momentum and efficiency

(15) $p_{2_t} - p_{1_t} = \eta \, \omega \, r \, \rho \, (w_{u_1} - w_{u_2})$

and may also be expressed using the Bernoulli equation as

(16) $p_{2_t} - p_{1_t} = p_2 - p_1 - \frac{\rho}{2} (w_{u_1}^{\;2} - w_{u_2}^{\;2}) + \omega \, r \, \rho \, (w_{u_1} - w_{u_2})$.

Substituting $p_{2_t} - p_{1_t}$ from Equation 15 into Equation 16,

(17) $p_2 - p_1 = \frac{1}{2} \rho \, (w_{u_1}^{\;2} - w_{u_2}^{\;2}) - (1 - \eta) \, \omega \, r \, (w_{u_1} - w_{u_2}) \, \rho$.

Substituting the expression for $p_2 - p_1$ as given in Equation 17 into Equation 14 and introducing

(18) $\Psi = 2 \xi \frac{w_{u_1} - w_{u_2}}{u_o}$,

$$(19) \quad \frac{w_{u_1}}{u_o} = \xi - \phi \tan \gamma_1 \quad ,$$

$$(20) \quad \frac{w_{u_1} + w_{u_2}}{2u_o} = \xi - \phi \tan \gamma_1 - \frac{\Psi}{4\xi} \quad ,$$

an expression for L/c equal to Δp is obtained for use in Equation 11:

$$(21) \quad \frac{L}{\frac{1}{2}\rho u_o{}^2 c} = \frac{\Delta p}{\frac{1}{2}\rho u_o{}^2} = \frac{s}{c}\,\frac{\phi}{\xi}\,\frac{1}{\cos \beta_\infty}\left[1 - (1-\eta)\,\frac{\xi \tan \beta_\infty \cos^2 \beta_\infty}{\phi}\right] ,$$

where $(1-\eta)$ may be determined from Equation 17 when evaluated at the tip radius as

$$(22) \quad 1 - \eta_o = \left[1 - \phi \tan \gamma_1 - \frac{\Psi}{4} - \frac{p_2 - p_1}{\frac{1}{2}\rho u_o{}^2}\,\frac{1}{\Psi}\right]_{\xi = 1}$$

and

$$(23) \quad \frac{1}{\cos \beta_{\infty_o}} = \left[1 + \left(\frac{1}{\phi} - \tan \gamma_1 - \frac{\Psi}{4\phi}\right)^2\right]^{\frac{1}{2}}_{\xi = 1}$$

$$(24) \quad \tan \beta_{\infty_o} \cos^2 \beta_{\infty_o} = \left[\frac{\frac{1}{\phi} - \tan \gamma_1 - \frac{\Psi}{4\phi}}{1 + \left(\frac{1}{\phi} - \tan \gamma_1 - \frac{\Psi}{4\phi}\right)^2}\right]_{\xi = 1} .$$

Since it has been shown that the work coefficient remains nearly constant with small changes in tip clearance, the decrease in efficiency, using Equation 11, is

$$(25) \quad \Delta E = 2\,\frac{c_o}{s}\,\frac{\delta}{R_o}\,\frac{K}{(1 - \xi_i{}^2)}\,\frac{1}{\Psi\,\phi}\left[\frac{\Delta p}{\frac{1}{2}\rho u_o{}^2}\right]^{3/2}$$

where $\Delta p/\frac{1}{2}\rho u_o^2$ is given by Equation 21.

To include the effect of pressure increase on the blade due to the impinging boundary layer flow, Rains evaluates Equation 7 at $y = \delta/2$, which gives

$$(26) \quad \frac{u_n}{u_o} \cong \left[\frac{\Delta p}{\frac{1}{2}\rho u_o^2} + \cos^2 \beta_o^{\,*} \, I\left(\frac{\delta}{2\delta^*}\right) \right]^{1/2}$$

and a corresponding drop in efficiency of

$$(27) \quad \Delta E = 2 \frac{c_o}{s} \frac{\delta}{R_o} \frac{K}{(1-\xi_i^2)} \frac{1}{\bar{\Psi} \bar{\phi}} \left[\frac{\Delta p}{\frac{1}{2}\rho u_o^2} + \cos^2 \beta_o^{\,*} \, I\left(\frac{\delta}{2\delta^*}\right) \right]^{3/2} .$$

To investigate the validity of the model above, calculations of change in efficiency and total pressure coefficient were made using the above relations. Experimental values obtained at the smallest tip clearance, $\lambda = 0.0025$, were used with the above equations to predict changes as tip clearance was increased. Values of ϕ_o and Ψ_o were obtained from Figures 12 and 17 respectively by neglecting the changes in the boundary layer region and extrapolating the slope in the mainstream to the tip radius. The absolute entering angles at the tip were obtained from Figures 25 - 29 in a manner similar to that described for ϕ_o and Ψ_o. The boundary layer displacement thickness was determined from Figure 30 to be $\delta^* = 0.068$ inches. A comparison was made of the losses obtained from a triangular pressure loading at the tip to that of a constant pressure loading using Equation 11, where the average pressure was the same in both cases and the vertex of the triangle was at the one-quarter chord. It was found that the ratio of the losses with triangular loading to those with constant loading was $K = 1.13$. Since it was felt that the triangular pressure distribution was a better representation of the loading, it was included in the calculations.

A comparison of calculated and experimental changes in total pressure coefficient and efficiency of the rotor are given in Table II and Figures 8 and 31. Rains' experimental values are also shown for comparison in Figure 31. A calculation of change in total pressure coefficient and efficiency of the rotor at the design flow rate using Rains' approximations (constant chordwise pressure loading, blade stagger angle at the tip and average values of ϕ and Ψ) is included in Table II.

As seen in the case of the change of work coefficient, it appears from the results of this experiment that inclusion of the scraping flow effect, handled in the manner described by Rains, leads to a prediction of excessive changes in total pressure coefficient and efficiency of the rotor with tip clearance. Though his tests were conducted at the design flow rate only, his experimental results agree very well with those predicted from calculation, as seen in Figure 31. The agreement between theory and experiment in this investigation is not as close as that found by Rains. However, the tests reported here cover a much larger range of flow rates and tip clearances than those of Rains, and their internal consistency indicates that they are as reliable as previous experiments. It is felt that the effect of the scraping flow would be reduced by taking into account the portion of the boundary layer flow that goes through the clearance, rather than assuming it all turned, as in shear flow into a corner.

Neglecting the scraping flow, it is seen from Table II that the change with flow rate of rotor efficiency drop due to tip clearance is overestimated near stall and underestimated at the high flow rate above design. Due to the scattering of experimental results and the small changes involved, i.e., most changes are not much more than the order of accuracy of the experimental set-up, it is felt that one can only discuss trends in evaluating the validity of the proposed model. In this respect, it is felt that the model is a valid one, since the order of magnitude of the losses is in reasonable agreement with the experimental results over a wide range of flow rates, and the variation in calculated and experimental efficiency drop with flow rate shows similar trends. In evaluating off-design performance, it is felt that local values of ϕ and Ψ at the tip must be considered rather than the average values over the radius. To describe accurately the flow through the tip clearance, three-dimensional effects should be considered, since the streamlines in the tip region are actually curved, giving a change in flow rate through the clearance. Two-dimensional flow was assumed in this analysis, and it is felt that with the scattering of experimental results the more elaborate three-dimensional analysis is not justified.

REFERENCES

1. Eckert, Bruno, "The Influence of the Radial Clearance of the Rotor on Compressor Efficiency: Part C" of The Influence of Physical Dimensions and Flow Conditions on Compressor Characteristics, U. S. Navy Bureau of Ships 338, pp. 95-108, (1946).

2. Rains, Dean A., "Tip Clearance Flows in Axial Flow Compressors and Pumps", California Institute of Technology, Hydrodynamics and Mechanical Engineering Laboratories, Report No. 5, Navy Contracts N6-ori-012, Task Order IV and NOrd 9612, (June 1954).

3. Ruden, P., "Investigations of Single Stage Axial Fans", NACA TM 1062 (1937).

4. Fuller, T. W. and Acosta, A. J., "Report on Design and Construction of the Axial Flow Pump Test Facility", Dept. of the Navy, Bureau of Ordnance, Contract NOrd 9612, Report No. E-12. 1. 3 (June 1953).

5. Rannie, W. D., Sabersky, Rolf H., and Bowen, John T., "Theoretical and Experimental Investigations of Axial Flow Compressors", Summary Report, California Institute of Technology, Mechanical Engineering Laboratories (January 1949).

6. Neustein, Joseph, "Experiments at Low Reynolds Number, Part II., Axial Flow Turbomachines", California Institute of Technology, Hydrodynamics and Mechanical Engineering Laboratories, Navy Contract Nonr-220(23), NR 097-001, Report No. 6 (March 1957).

7. Wu, Chung-Hua, "Survey of Available Information on Internal Flow Losses Through Axial Turbomachines", NACA RM E50J13 (1951).

8. Milne-Thompson, L. M., Theoretical Hydrodynamics, McMillan, 2nd Edition (1950).

APPENDIX A

Notation

b	Blade height
c	Blade chord
c_a	Absolute axial velocity
c_u	Absolute tangential velocity
p	Static pressure
r	Radius
s	Blade spacing
t	Time
u, v	Velocity
u_n	Tip clearance velocity normal to the blade chord
u_o	Tip rotative speed
w	Velocity relative to the blade
x, y, z	Coordinates
D	Diameter
E	Efficiency
I	Pressure distribution function
N	Number of blades
P	Power
Q	Volume flow rate
R_i	Hub radius in the machine
R_o	Tip radius in the machine
R_p	Reynolds number, $u D_o/\nu$ based on flow velocity at nozzle exit
T	Torque
U, V	Velocities

W	Work
β	Relative flow angle (measured from machine axis)
β^*	Stagger angle of rotor row (angle between chord line and machine axis)
β_∞	Mean relative flow angle
γ	Absolute flow angle (measured from machine axis)
δ	Tip clearance
δ^*	Displacement thickness of boundary layer
η	Local efficiency
λ	Dimensionless tip clearance δ/b
ω	Rotational frequency
Δ	Change in any quantity
ξ	Radius ratio, r/R_o
μ	Viscosity
ρ	Density
ν	Kinematic viscosity, μ/ρ
ϕ	Flow rate coefficient = $\frac{\text{axial velocity}}{\text{tip speed}}$
$\bar{\phi}$	Integrated average flow rate coefficient
ψ	Total head coefficient = local total heat rise across the rotor/ $\frac{1}{2}\rho u_o^2$
$\bar{\psi}$	Integrated average total head coefficient
Ψ	Local work coefficient = $2\xi \frac{c_{u1} - c_{u2}}{u_o}$
$\bar{\Psi}$	Average work coefficient = $T/\rho(u_o^2/2)R_o\Omega$

Subscripts

∞	Mean value
o	Value at rotor blade tip
1	Value just ahead of the rotor
2	Value just behind rotor

APPENDIX B

Comparison of Rotor Entering and Leaving Angles

Since detailed surveys of flow through the rotor were made, it is interesting to examine the dependence of exit flow direction relative to the rotor as a function of inlet relative flow. For very high solidity, the exit flow direction relative to the rotor should be constant. As can be seen from the table below, there is considerable variation at mid-blade height for the flow rate near stall, and only small variations outside the stall region.

Comparison of Figures 25, 26, 27, 28, and 29 show no appreciable change in absolute entering angle with flow rate, other than a wake of varying intensity near radius ratio $\xi = 0.7$. The change in flow direction through the rotor, at mid-blade height using the center streamline as an approximate average is given below where $\beta_{2_{cal}}$ was determined using thin airfoil cascade theory:

$\bar{\Phi}$	$(\gamma_2-\gamma_1)^\circ$	β_1°	β_2°	$\beta_{2_{cal}}^\circ$
0.348	29°	$61^\circ 40'$	$43^\circ 45'$	$40^\circ 45'$
0.399	26°	$57^\circ 50'$	$40^\circ 45'$	$40^\circ 15'$
0.443	21°	$53^\circ 00'$	$39^\circ 20'$	$39^\circ 30'$
0.498	17°	$49^\circ 45'$	$38^\circ 10'$	$39^\circ 05'$
0.548	11.5°	$45^\circ 50'$	$37^\circ 30'$	$38^\circ 45'$

The relative entering and leaving angles are also compared at $\xi = 0.7$ and 0.9:

Φ	$\xi = 0.7$			$\xi = 0.9$		
	β_1	β_2	$\beta_{2_{cal}}$	β_1	β_2	$\beta_{2_{cal}}$
0.348	57°10'	26°30'	24°10'	65°00'	53°30'	51°15'
0.399	51°20'	26°15'	23°40'	61°00'	50°30'	50°15'
0.443	46°30'	24°30'	23°10'	58°00'	50°45'	49°40'
0.498	41°00'	22°15'	22°50'	54°40'	49°00'	49°10'
0.548	38°15'	22°00'	22°40'	51°50'	47°45'	48°40'

Both the absolute entering and leaving angle decrease from root to tip with similar slope, while the relative leaving angle, also plotted in Figs. 25-29, increases from root to tip.

TABLE I

Comparison of Experimental and Calculated Reduction in Work Coefficient

$\frac{\Delta \bar{\Psi}}{\bar{\Psi}}$ $\lambda = 0$ to $\lambda = 0.0254$					
Calculated					Experiment
$\bar{\phi}$	Eq. 3	Eq. 6	Eq. 9	Eq. (3+9)	
.343	.0365	.0447	.0152	.0517	.010
.40	.0354	.0433	.0150	.0504	.012
.45	.0285	.0348	.0159	.0444	.014
.50	.0262	.0320	.0180	.0442	.017
.55	.0207	.0254	.0229	.0436	.024

Equation 3 - Reduction due to physical tip clearance.

$$\frac{\Delta \bar{\Psi}}{\bar{\Psi}} = \frac{\phi_o}{\bar{\phi}} \frac{\Psi_o}{\bar{\Psi}} \frac{\delta}{b}$$

Equation 6 - Reduction due to physical tip clearance and flow into sharp-edged orifice.

$$\frac{\Delta \bar{\Psi}}{\bar{\Psi}} = \frac{2\pi}{\pi + 2} \frac{\phi_o}{\bar{\phi}} \frac{\Psi_o}{\bar{\Psi}} \frac{\delta}{b}$$

Equation 9 - Reduction due to "scraping up" of boundary layer.

$$\frac{\Delta \bar{\Psi}}{\bar{\Psi}} = \frac{2c_o}{s} \frac{\delta*}{R_o} \frac{\cos^3 \beta_o^*}{(1-\xi_i^2)} \frac{1}{\bar{\phi}\,\bar{\Psi}} \left[-\frac{\delta}{\delta*} + \frac{1}{3}\left(\frac{\delta}{\delta*}\right)^3 - \frac{1}{8}\left(\frac{\delta}{\delta*}\right)^4 + \frac{1}{80}\left(\frac{\delta}{\delta*}\right)^5 \right]$$

TABLE II

Comparison of Experimental and Calculated Reduction in Pressure Coefficient and Efficiency

$\Delta \bar{\Psi}_{\lambda = 0 \text{ to } \lambda = 0.0254}$					
	Calculated Without Scraping			Calculated With Scraping	
$\bar{\phi}$	$\bar{\Psi}$ x Eq. 25	Rains(2)	Experiment	Ψ x Eq. 27	Rains(2)
0.343	.034	.014	.025	.055	.027
0.40	.025		.025	.043	
0.45	.018		.020	.032	
0.50	.012		.015	.023	
0.55	.005		.010	.015	

$\Delta E_{\lambda = 0 \text{ to } \lambda = 0.0254}$					
	Calculated Without Scraping			Calculated With Scraping	
$\bar{\phi}$	Eq. 25	Rains(2)	Experiment	Eq. 27	Rains(2)
0.343	.068	.039	.047	.110	.073
0.40	.058		.047	.099	
0.45	.049		.046	.089	
0.50	.040		.040	.081	
0.55	.026		.037	.071	

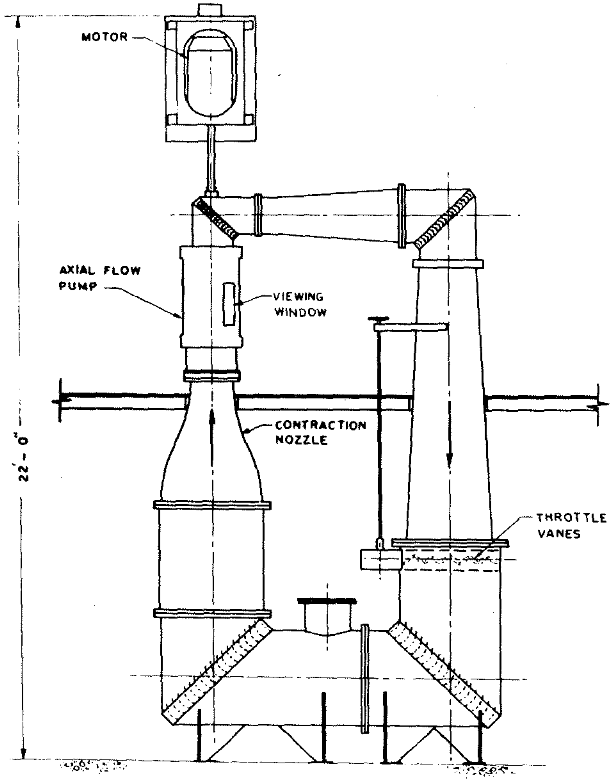

Fig. 1. Schematic Diagram of the Pump Circuit

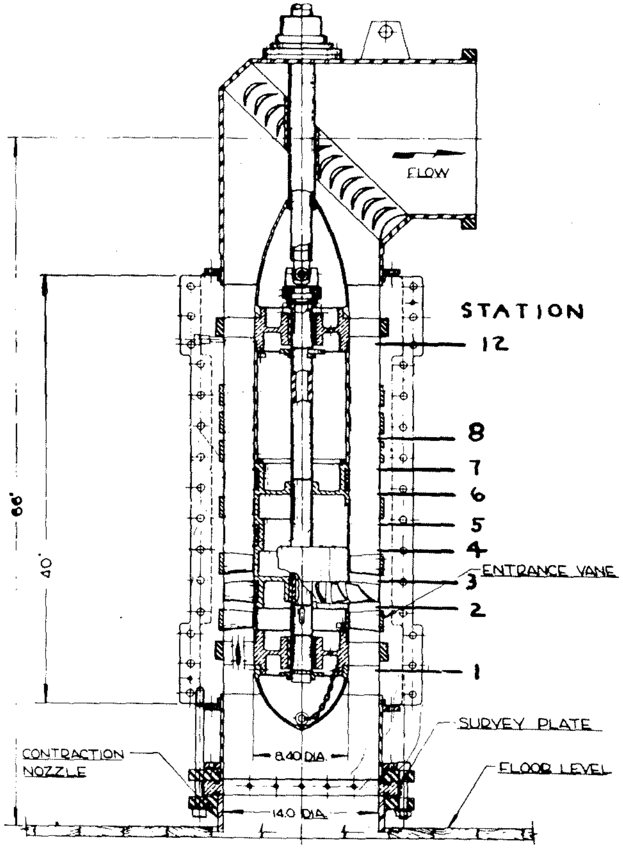

Fig. 2. Turbomachine Unit Showing Measuring Stations

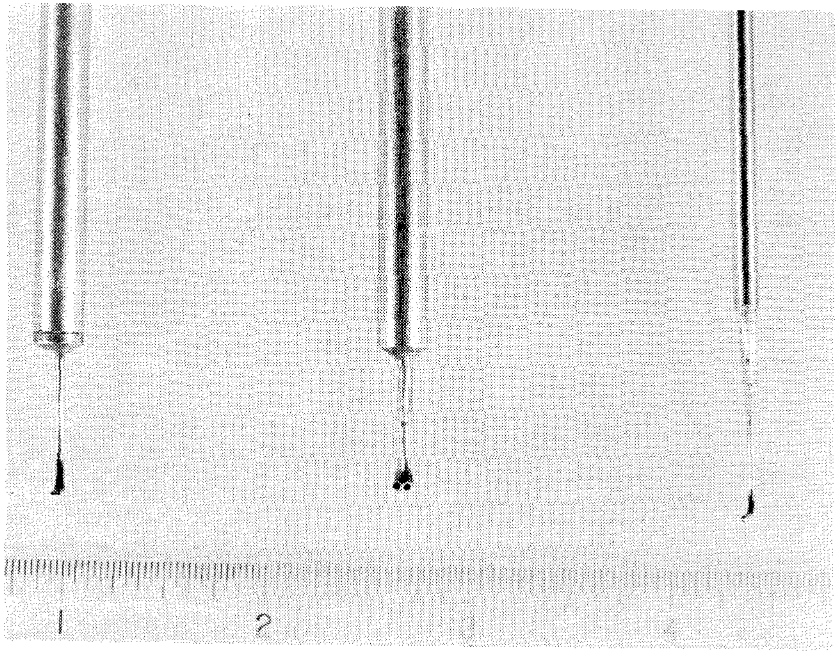

Fig. 3. Flow Measuring Instruments

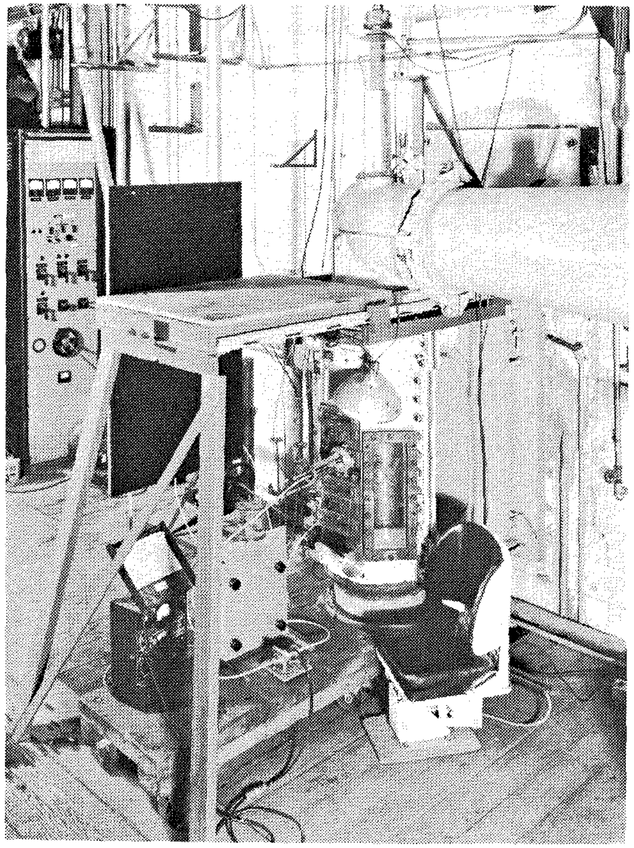

Fig. 4. Test Floor of the Pump Circuit

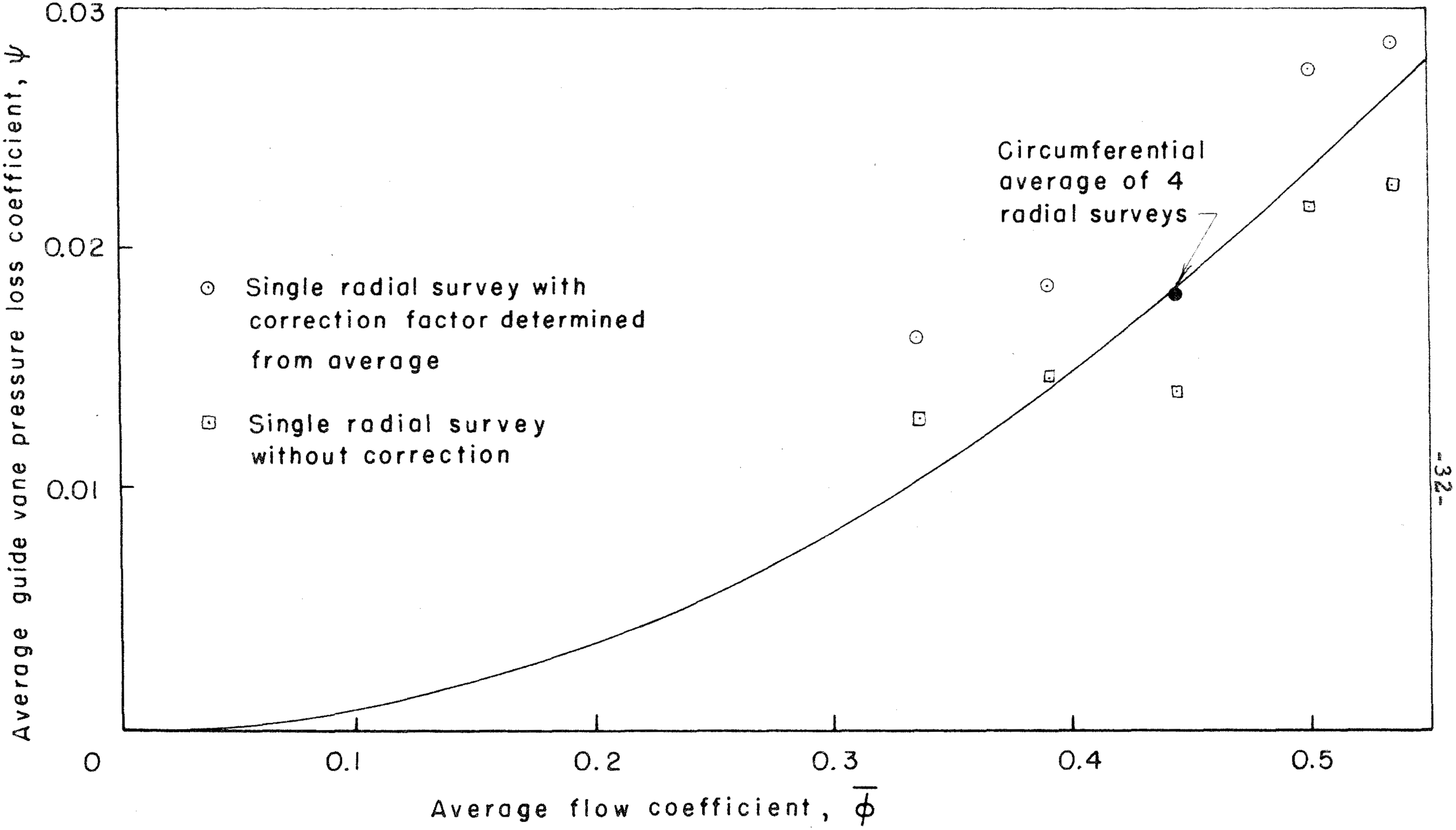

FIG. 5 - AVERAGE GUIDE VANE PRESSURE LOSS AS A FUNCTION OF AVERAGE FLOW COEFFICIENT

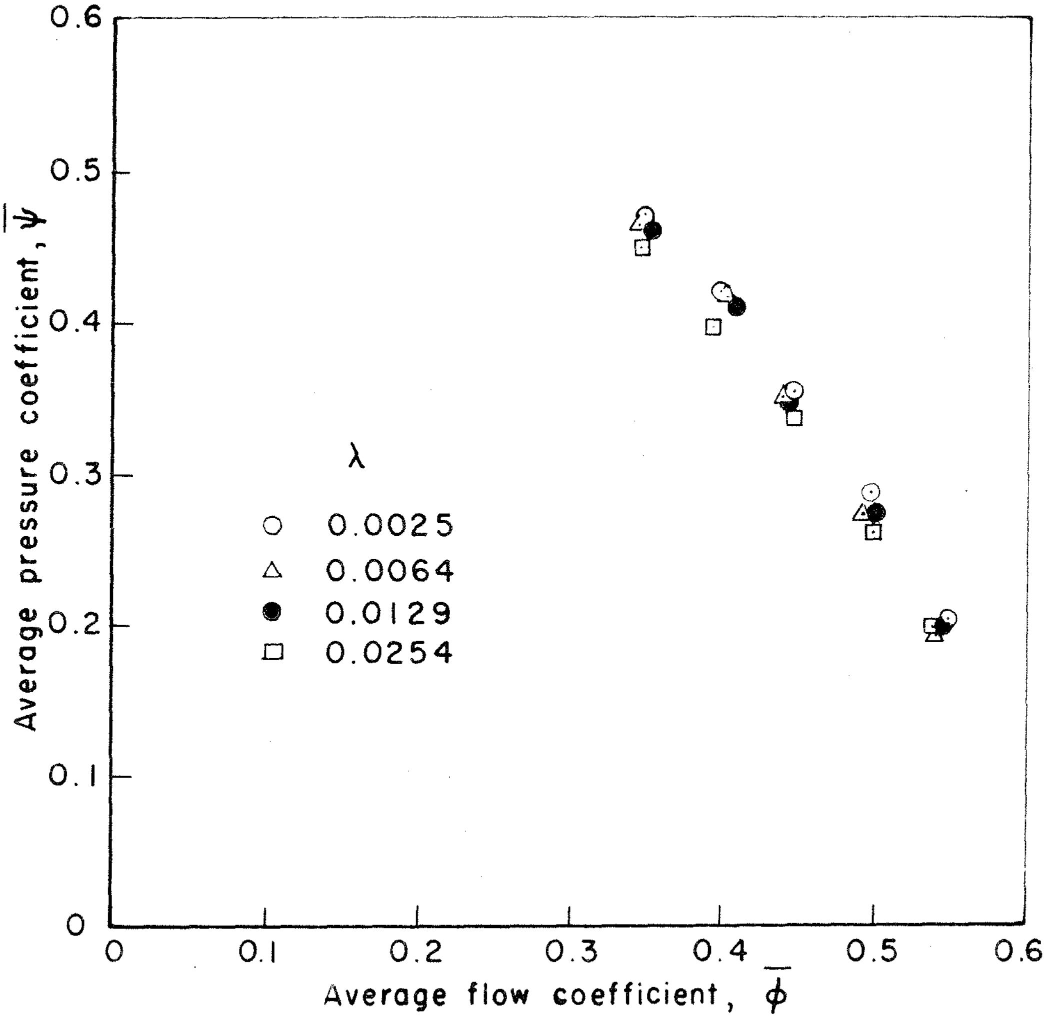

FIG. 6 AVERAGE PRESSURE COEFFICIENT VERSUS AVERAGE FLOW COEFFICIENT FOR VARIOUS TIP CLEARANCES

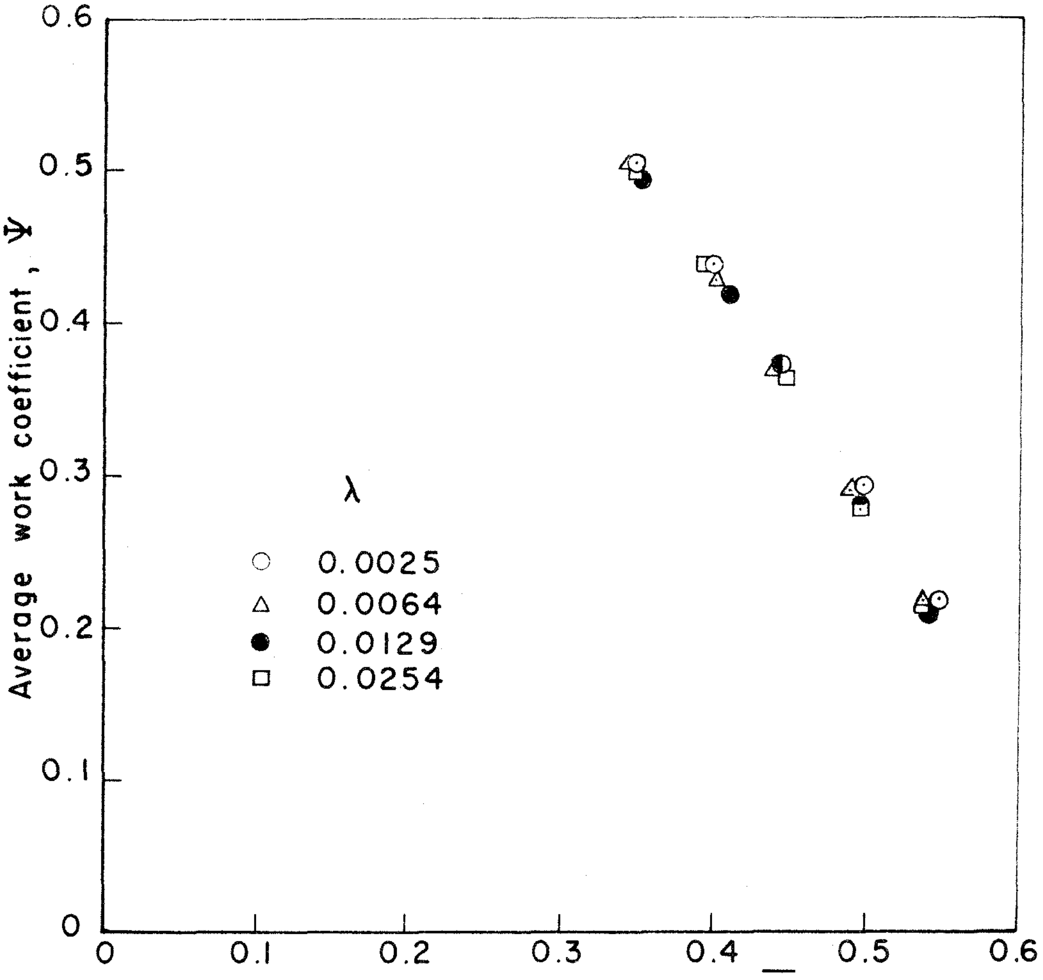

FIG. 7 AVERAGE WORK COEFFICIENT VERSUS AVERAGE FLOW COEFFICIENT FOR VARIOUS TIP CLEARANCES

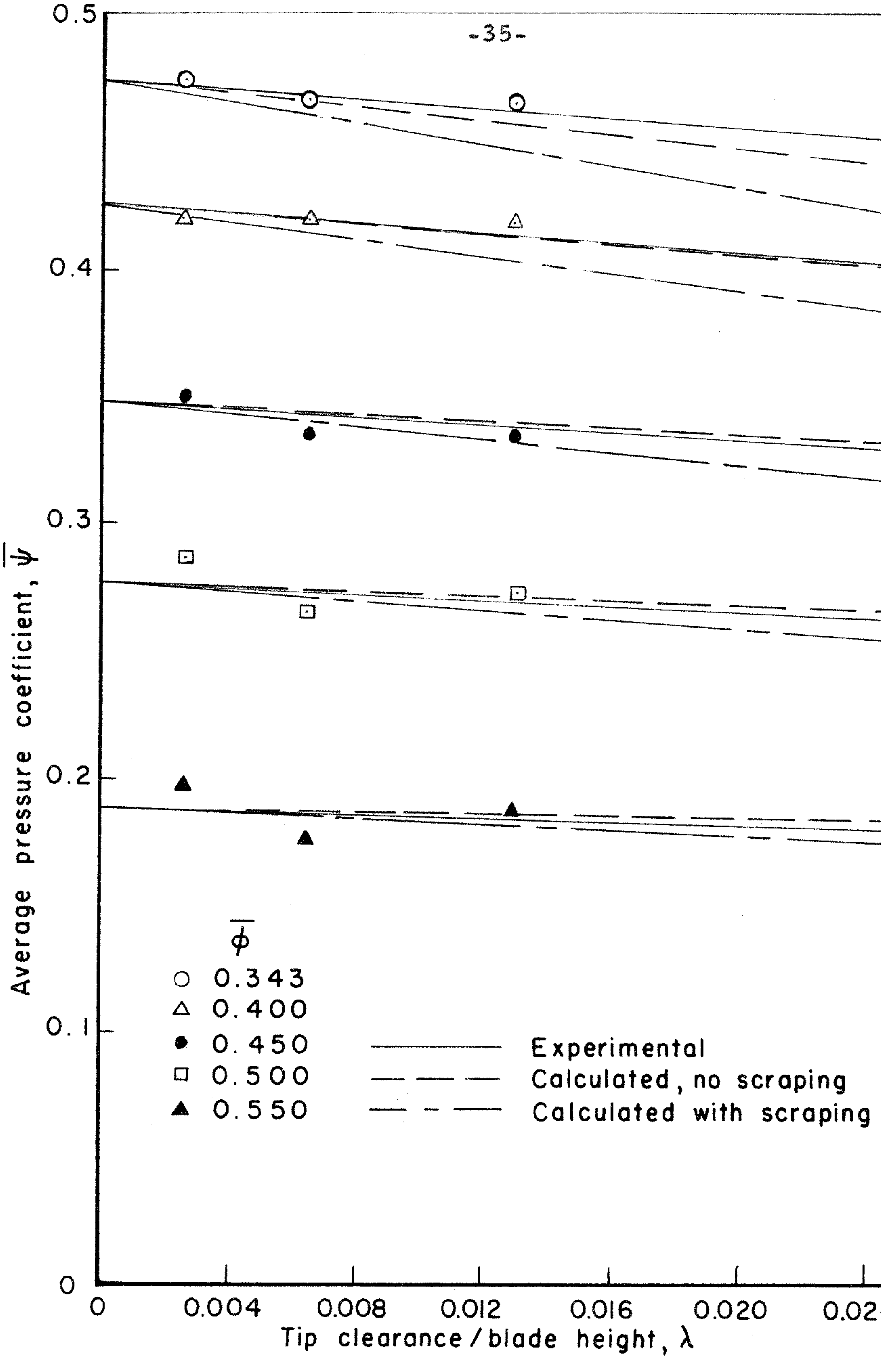

FIG. 8 AVERAGE PRESSURE COEFFICIENT AS A FUNCTION OF TIP CLEARANCE FOR VARIOUS FLOW RATES

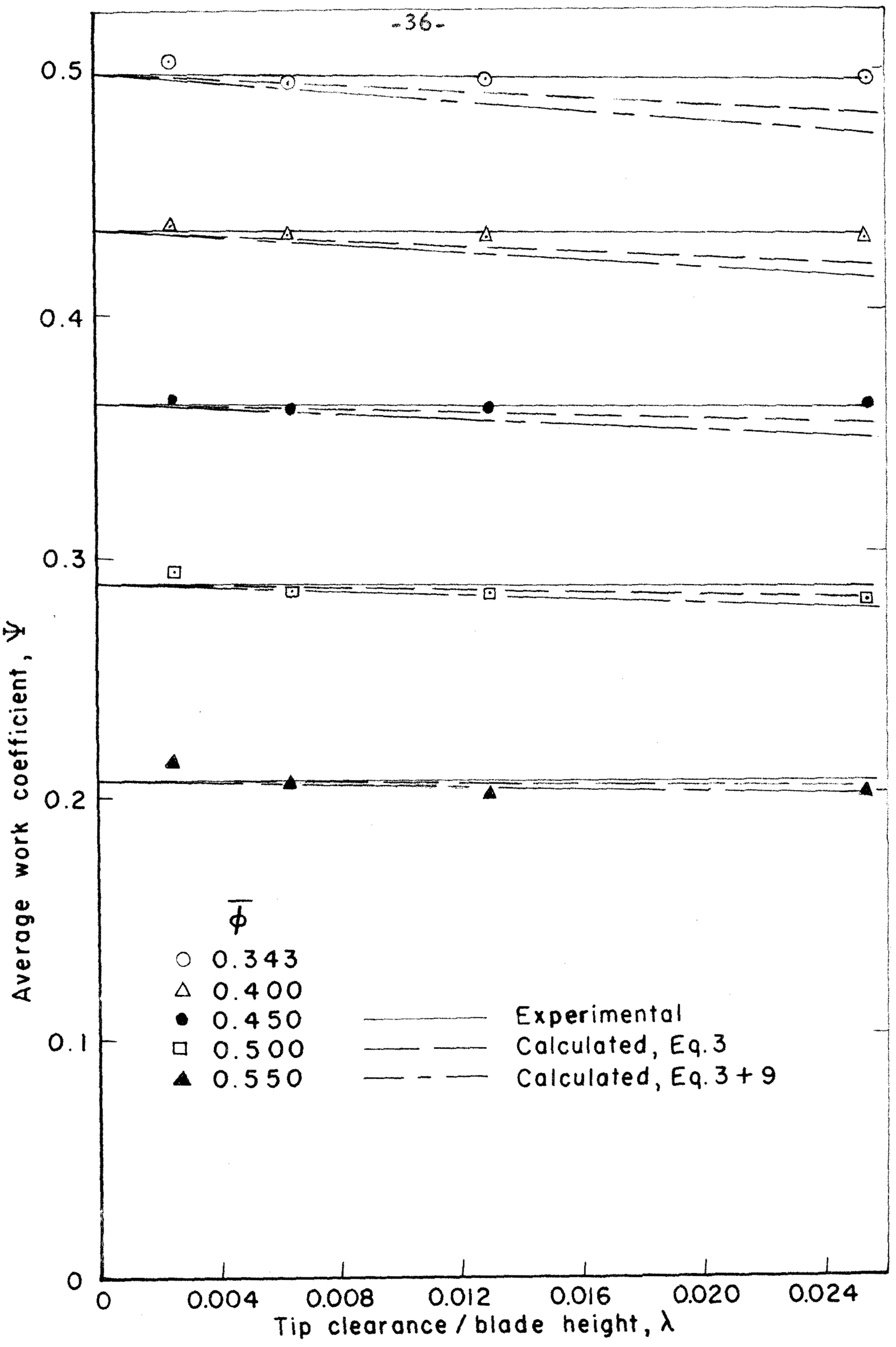

FIG. 9 AVERAGE WORK COEFFICIENT AS A FUNCTION OF TIP CLEARANCE FOR VARIOUS FLOW RATES

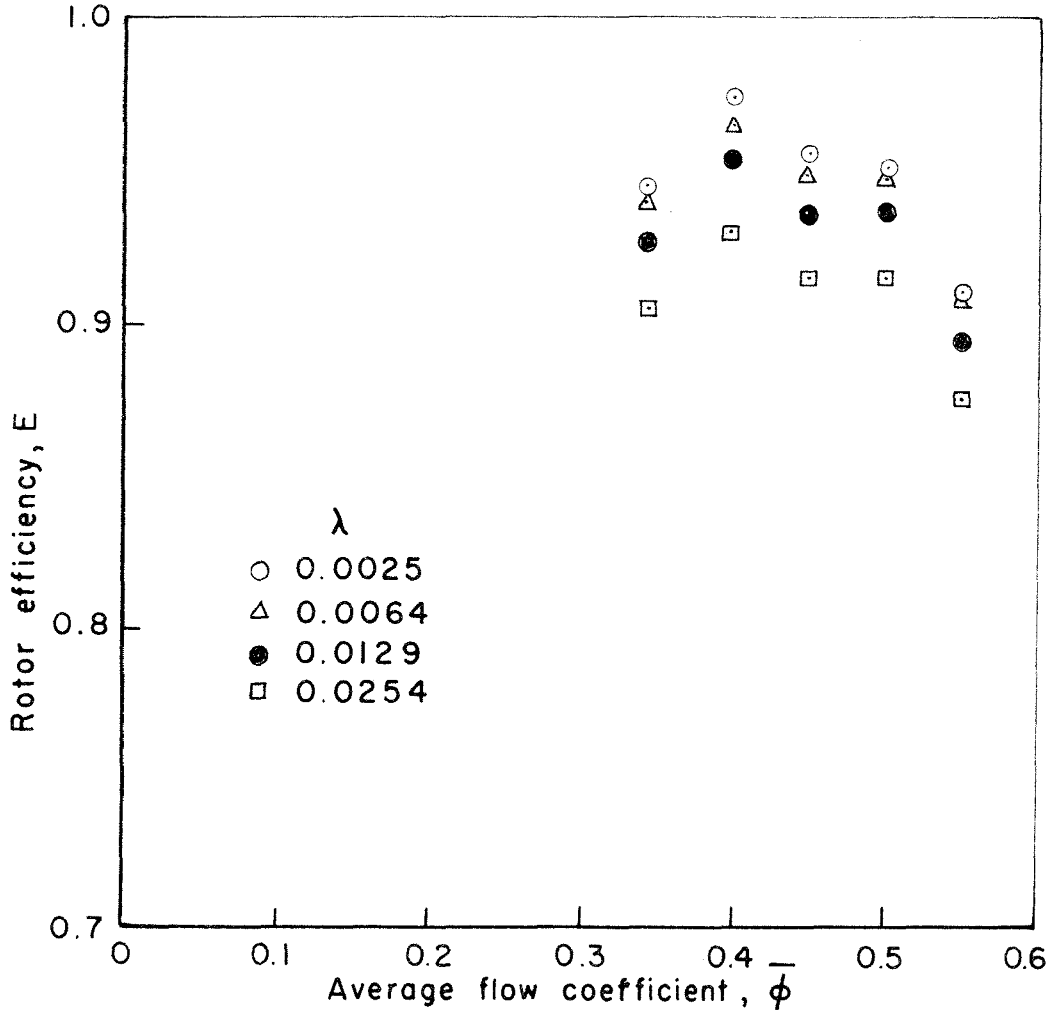

FIG. 10 ROTOR EFFICIENCY AS A FUNCTION OF AVERAGE FLOW COEFFICIENT FOR VARIOUS TIP CLEARANCES

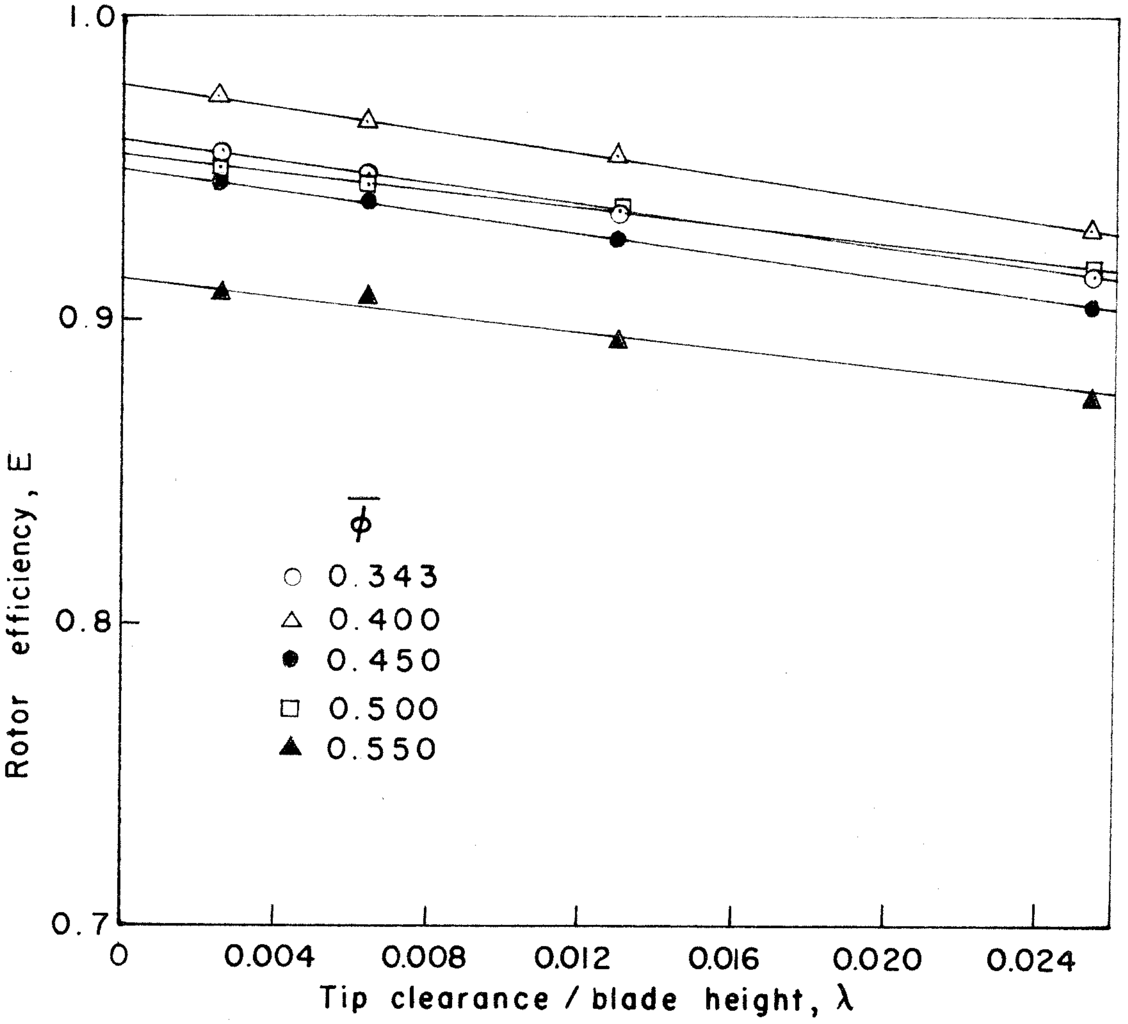

FIG. 11 ROTOR EFFICIENCY AS A FUNCTION OF TIP CLEARANCE FOR VARIOUS FLOW RATES

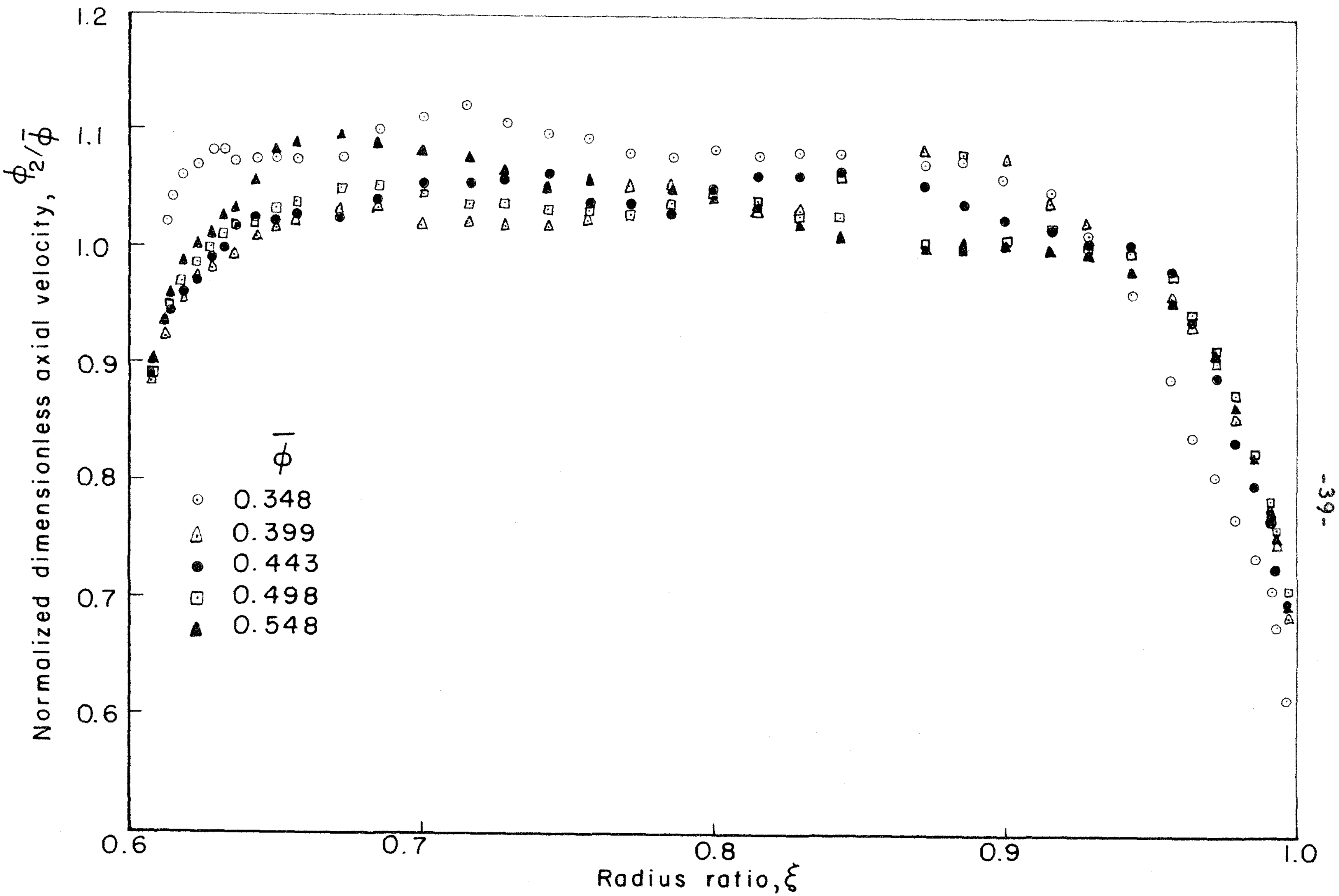

FIG. 12 - AXIAL VELOCITY SURVEYS BEHIND THE ROTOR FOR VARIOUS FLOW RATES AND $\lambda = 0.0025$

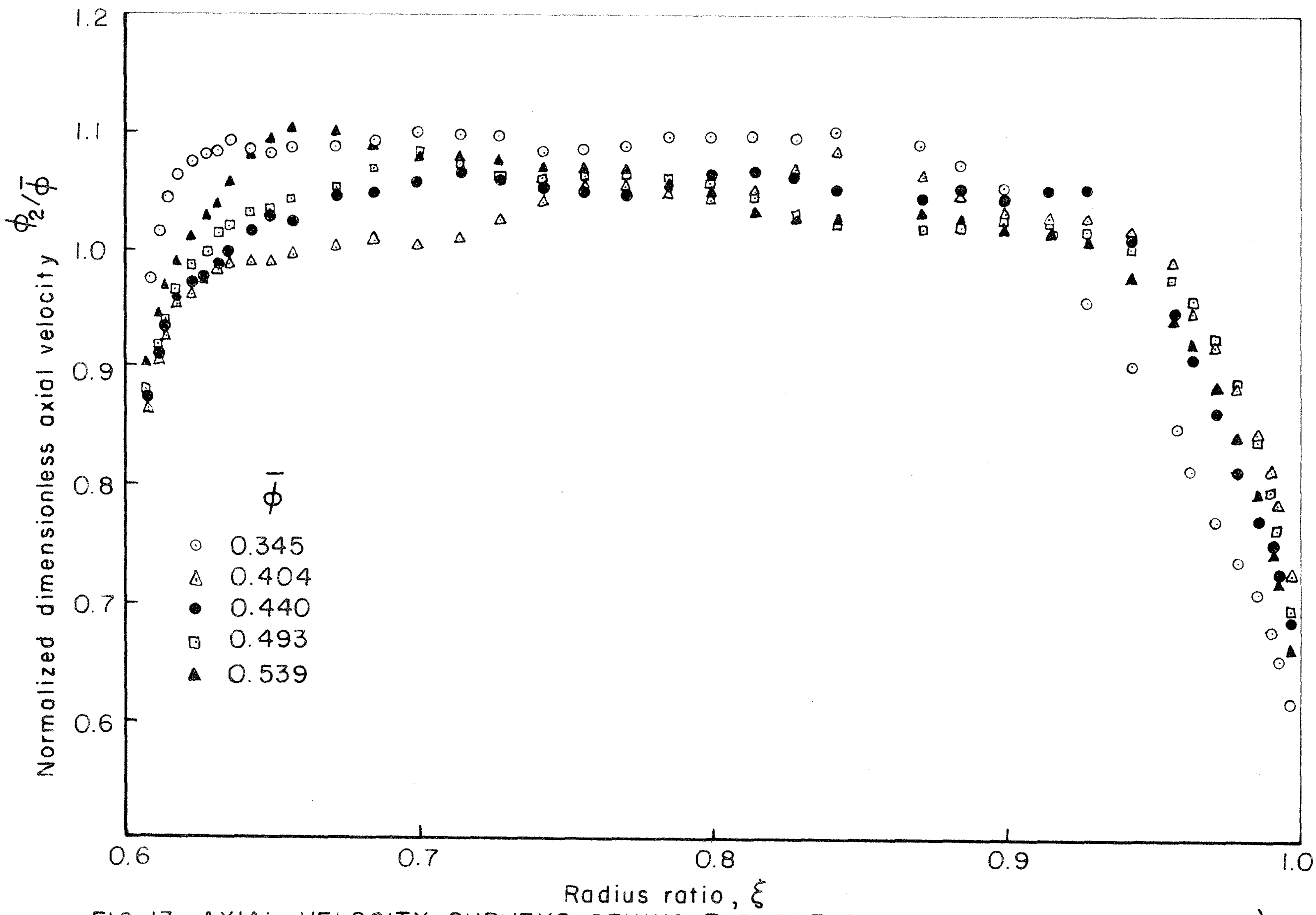

FIG. 13 - AXIAL VELOCITY SURVEYS BEHIND THE ROTOR FOR VARIOUS FLOW RATES, λ=0.0064

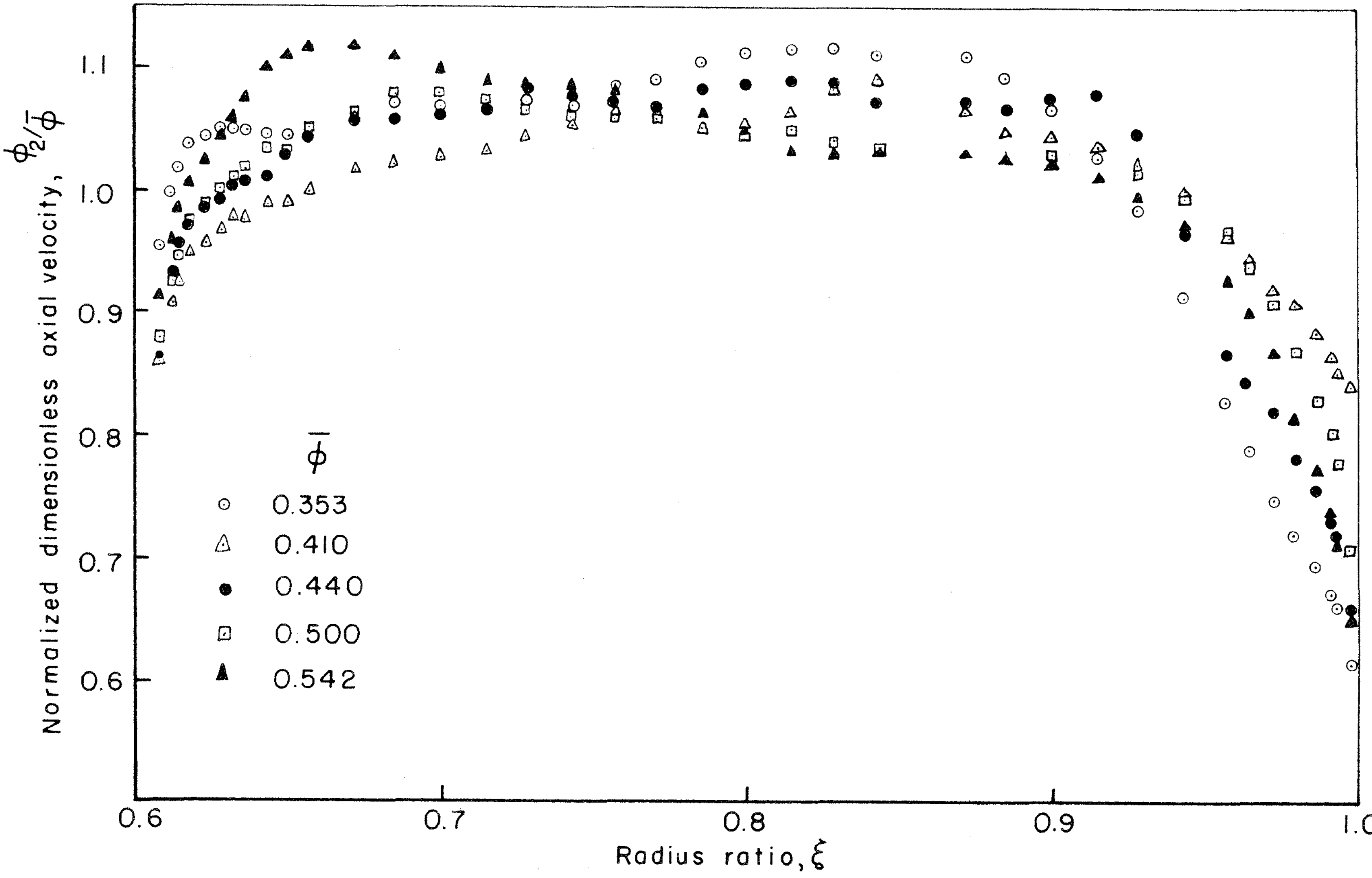

FIG. 14 – AXIAL VELOCITY SURVEYS BEHIND THE ROTOR FOR VARIOUS FLOW RATES, $\lambda = 0.0129$

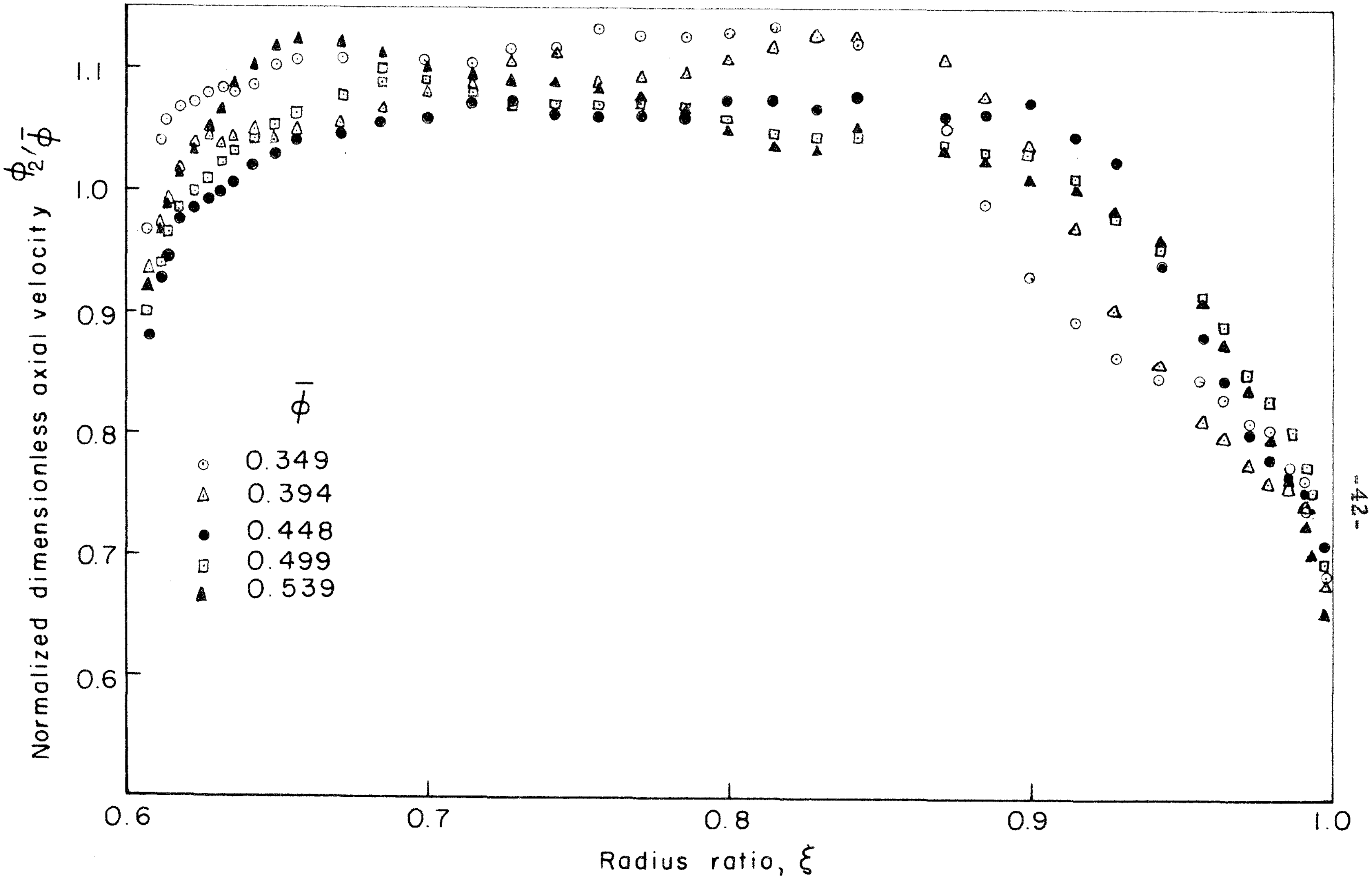

FIG. 15 - AXIAL VELOCITY SURVEYS BEHIND THE ROTOR FOR VARIOUS FLOW RATES, $\lambda = 0.0254$

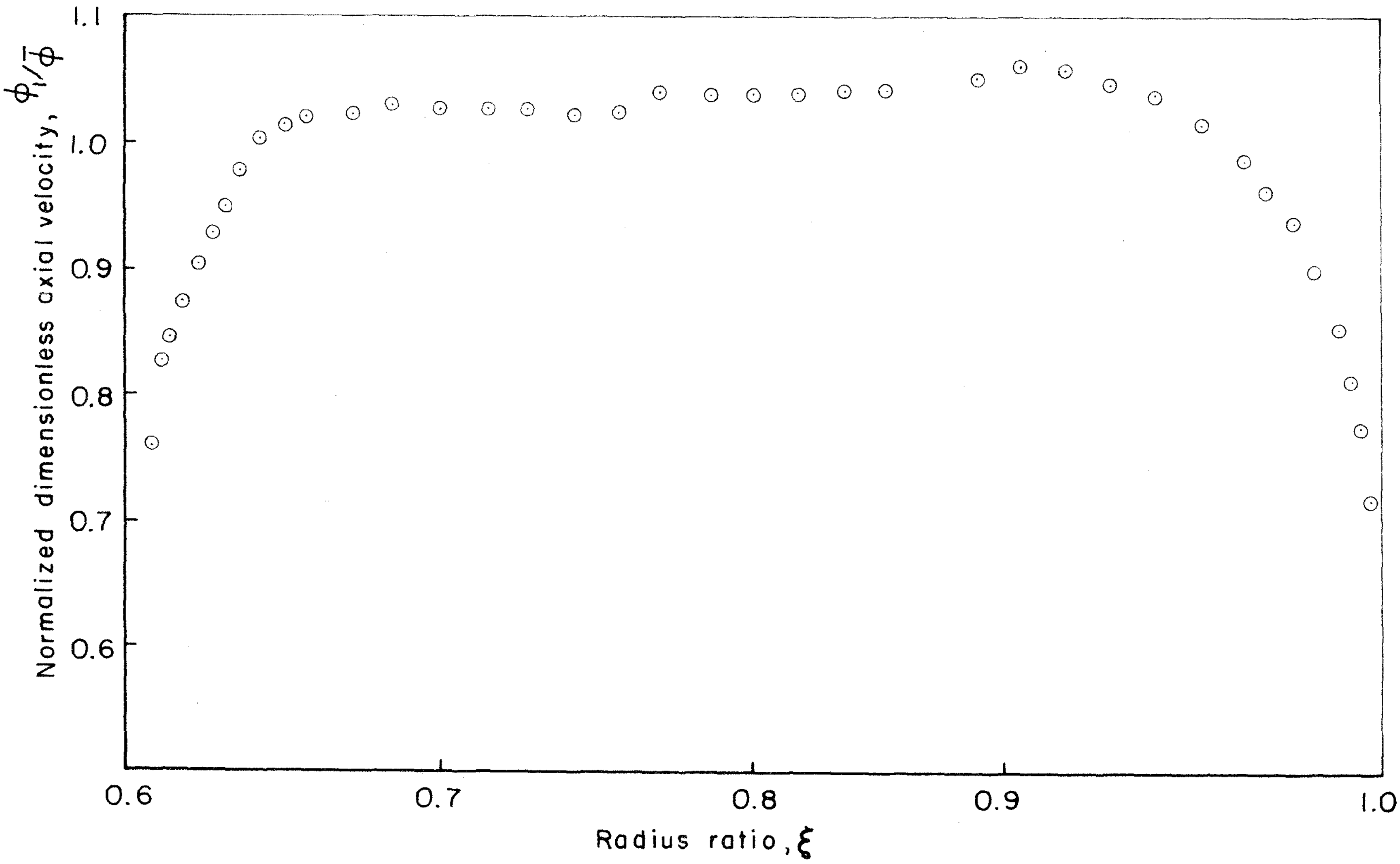

FIG. 16 – AXIAL VELOCITY SURVEY AHEAD OF THE ROTOR AVERAGED OVER FOUR CIRCUMFERENTIAL STATIONS, $\lambda = 0.0025$

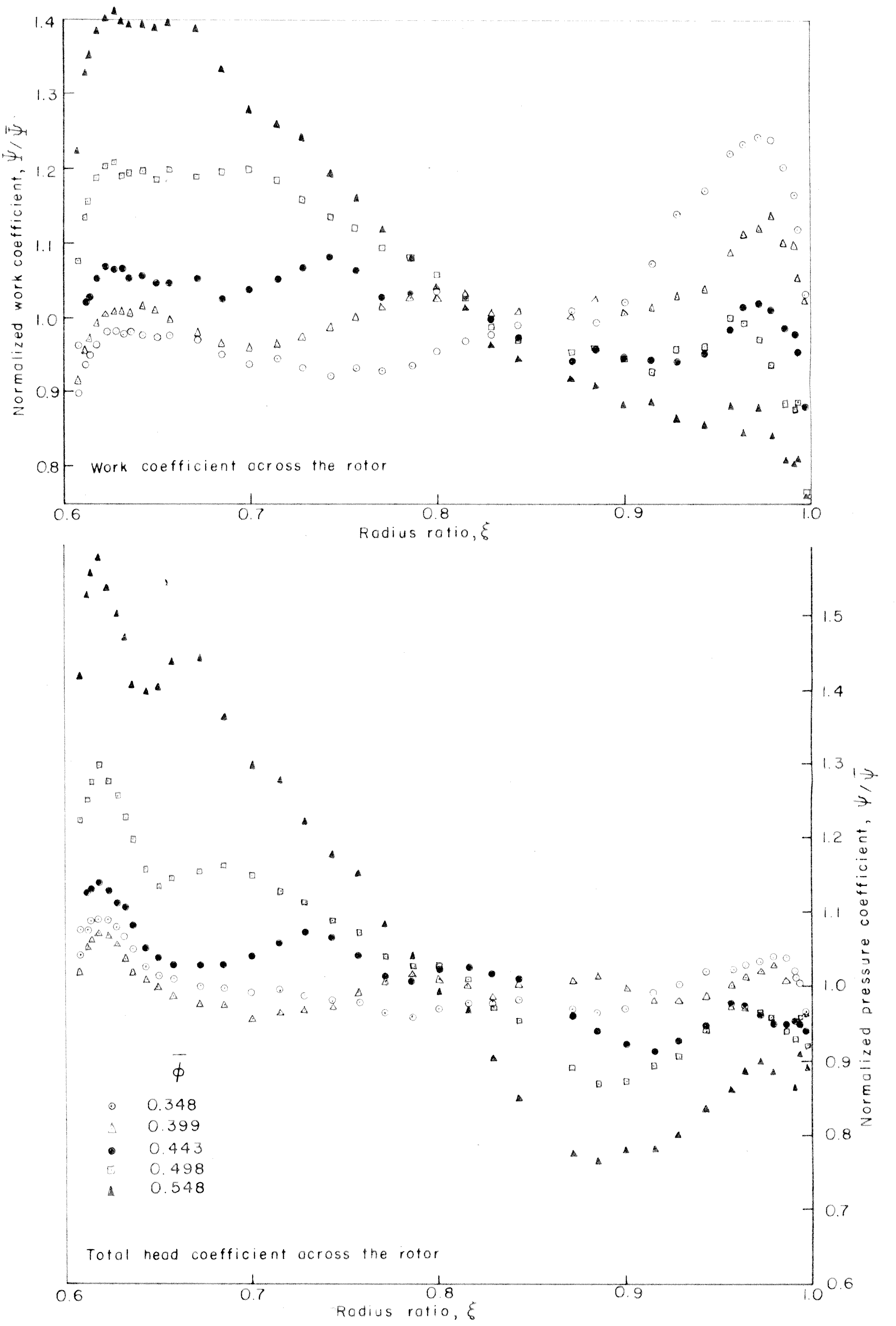

FIG. 17 — WORK COEFFICIENT AND TOTAL HEAD COEFFICIENT ACROSS THE ROTOR AS A FUNCTION OF RADIUS FOR VARIOUS FLOW RATES, $\lambda = 0.0025$

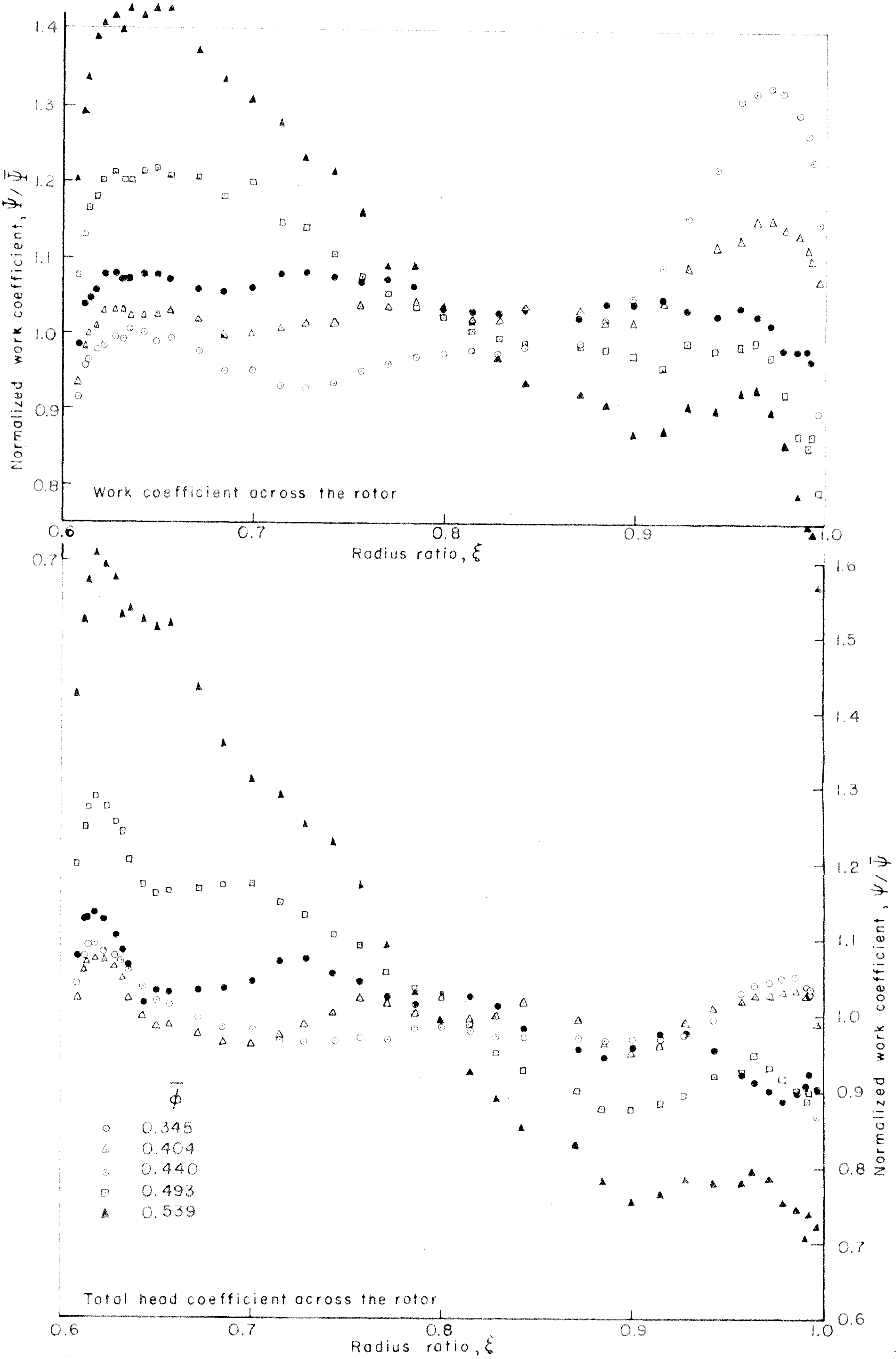

FIG. 18 - RADIAL DISTRIBUTION OF WORK COEFFICIENT AND TOTAL HEAD COEFFICIENTS ACROSS THE ROTOR AT VARIOUS FLOW RATES, λ = 0.0064

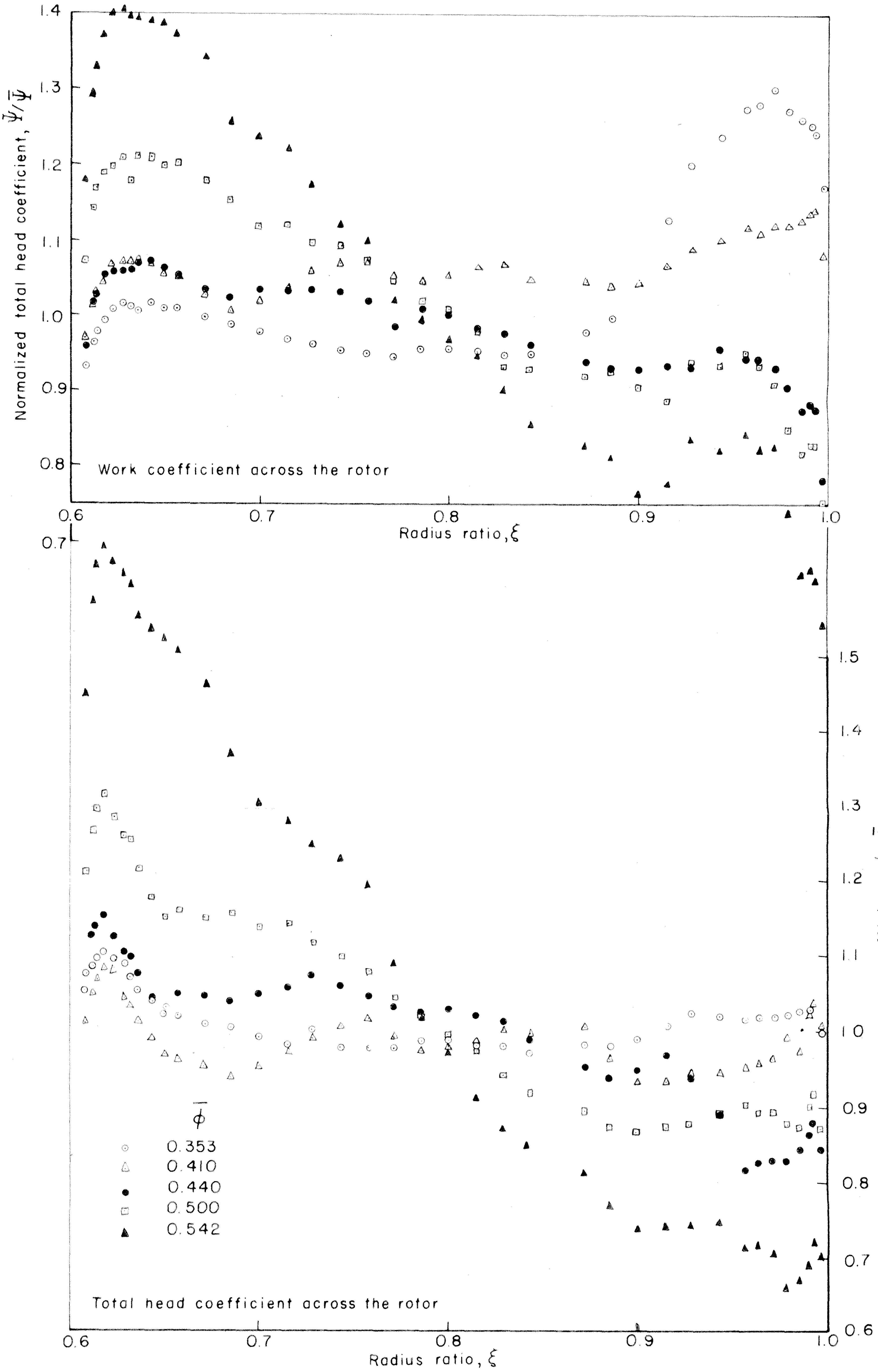

FIG. 19 - RADIAL DISTRIBUTION OF WORK COEFFICIENT AND TOTAL HEAD COEFFICIENT ACROSS THE ROTOR AT VARIOUS FLOW RATES, λ =0.0129

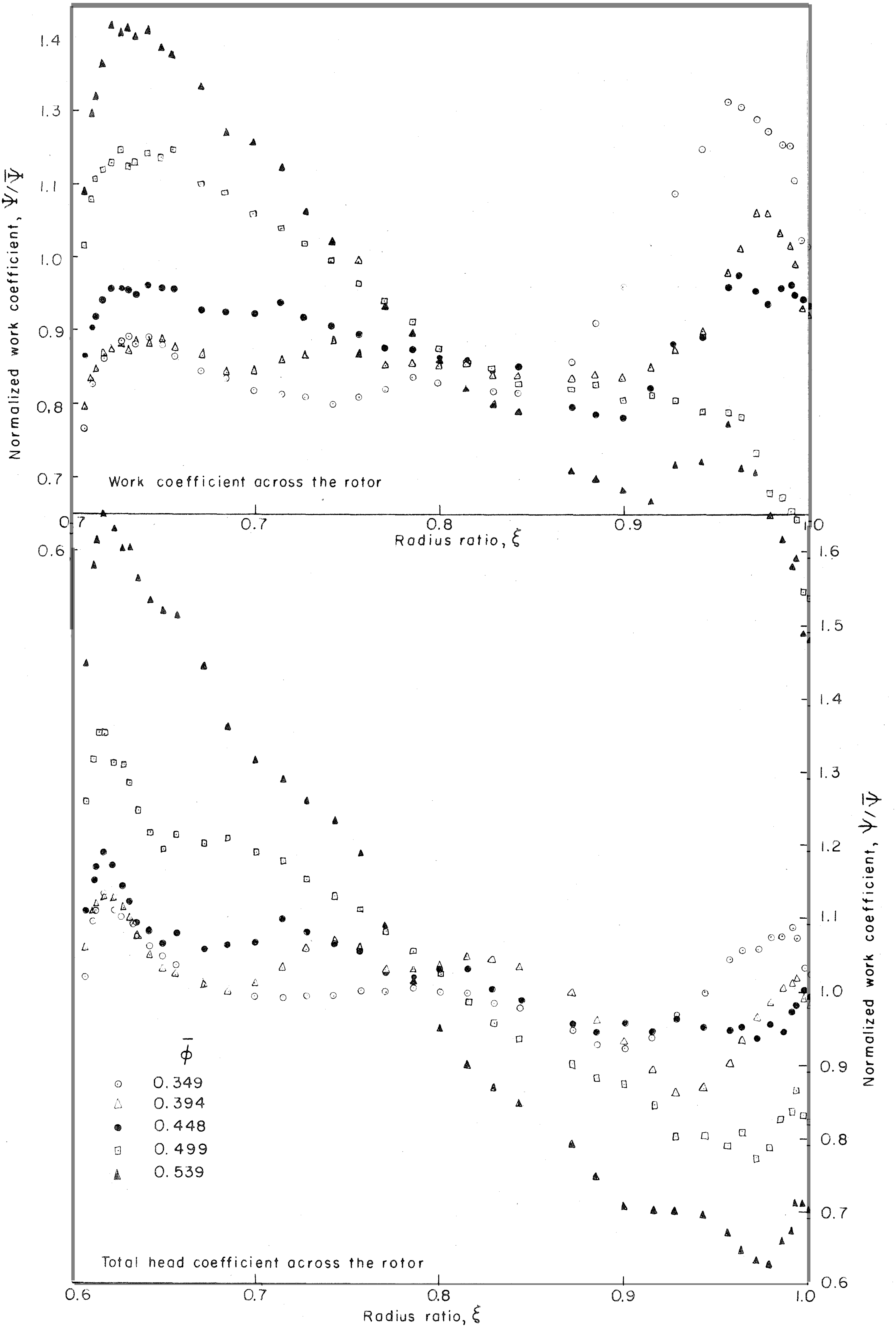

FIG.20- RADIAL DISTRIBUTION OF WORK COEFFICIENT AND TOTAL HEAD COEFFICIENT ACROSS THE ROTOR AT VARIOUS FLOW RATES, $\lambda = 0.0254$

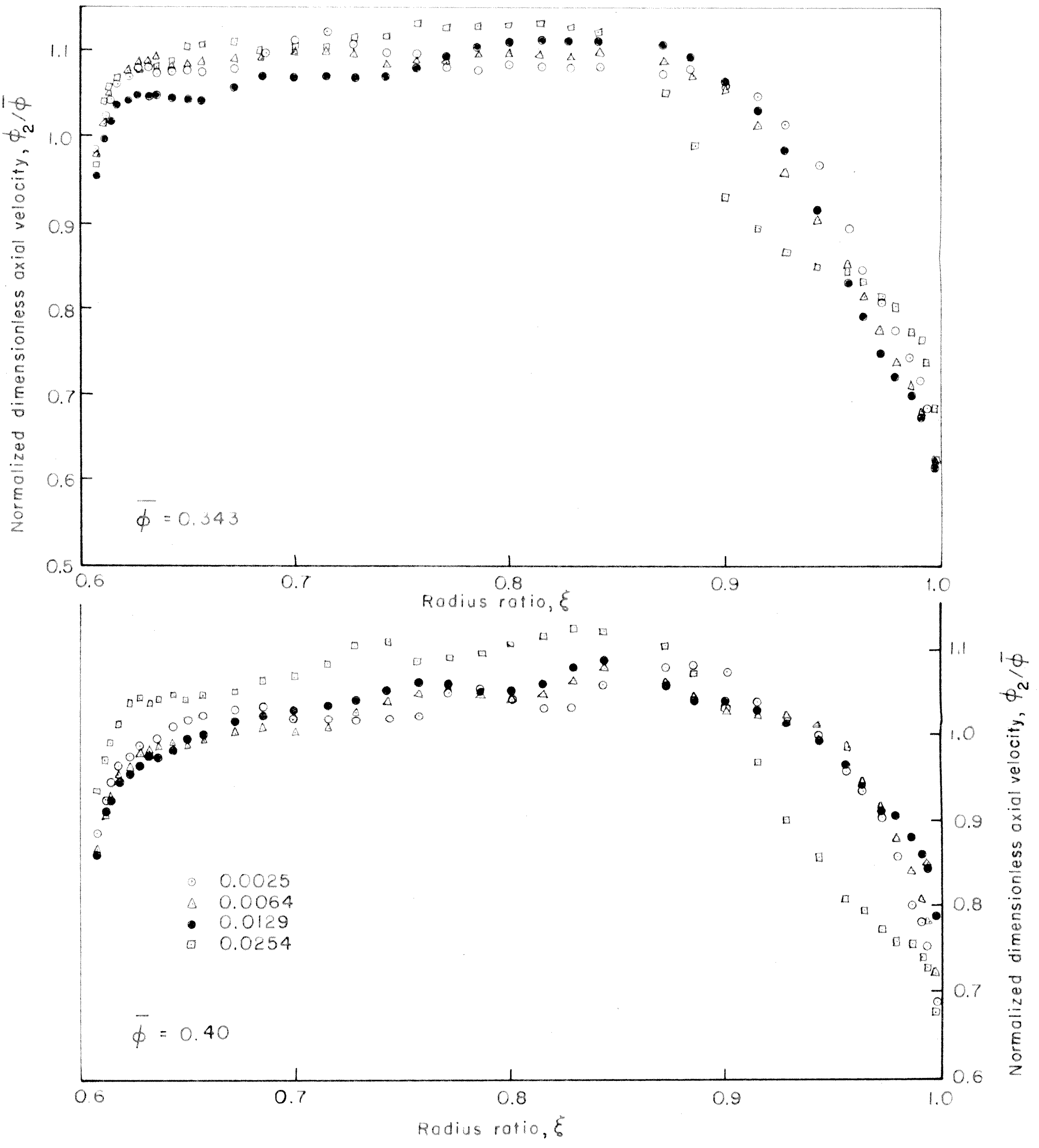

FIG. 21 - AXIAL VELOCITY BEHIND THE ROTOR FOR VARIOUS FLOW RATES AND TIP CLEARANCES

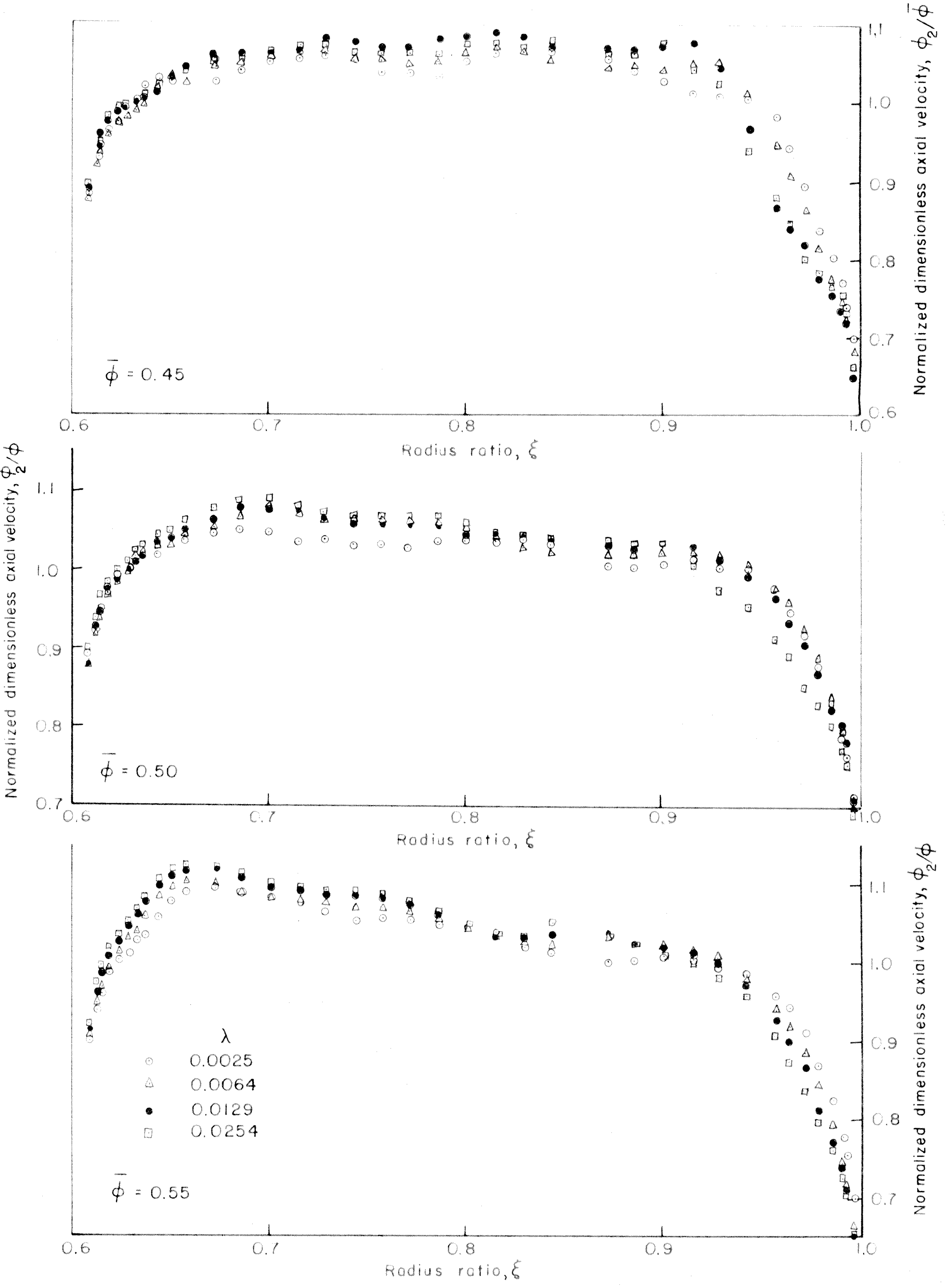

FIG. 21a – AXIAL VELOCITY BEHIND THE ROTOR FOR VARIOUS FLOW RATES AND TIP CLEARANCES

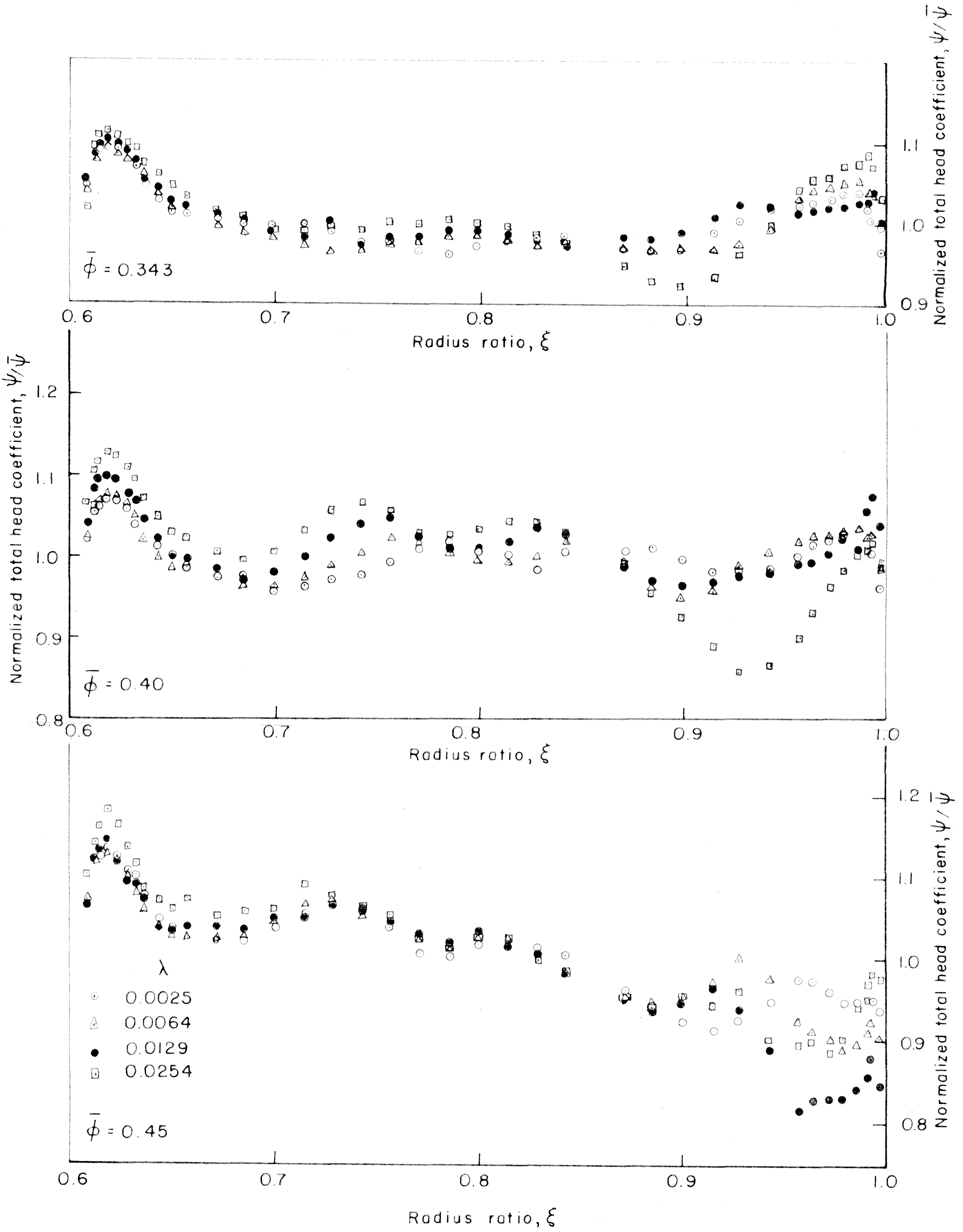

FIG. 22 - TOTAL HEAD COEFFICIENT ACROSS THE ROTOR FOR VARIOUS FLOW RATES AND TIP CLEARANCES

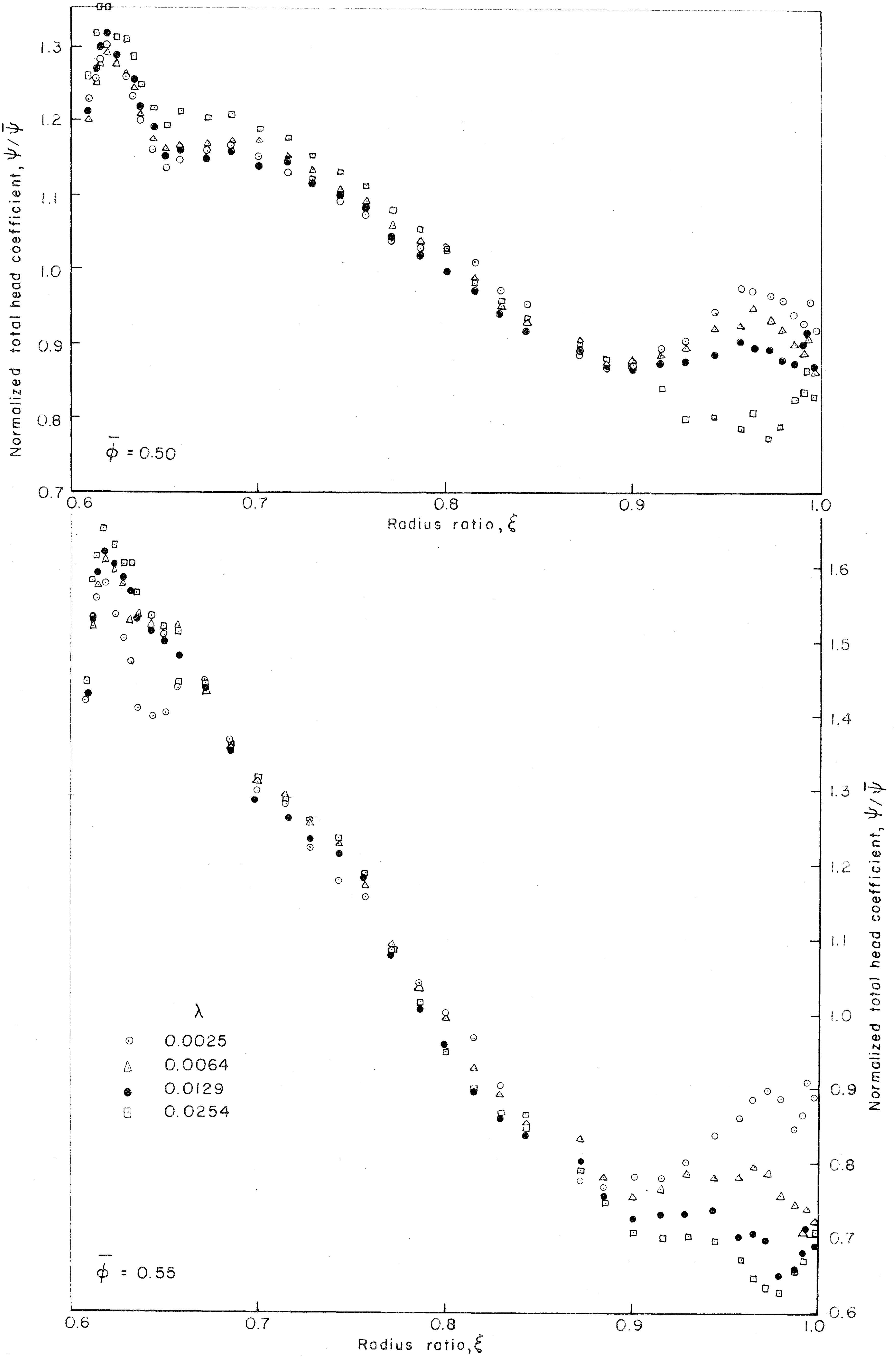

FIG. 22 a — TOTAL HEAD COEFFICIENT ACROSS THE ROTOR FOR VARIOUS FLOW RATES AND TIP CLEARANCES

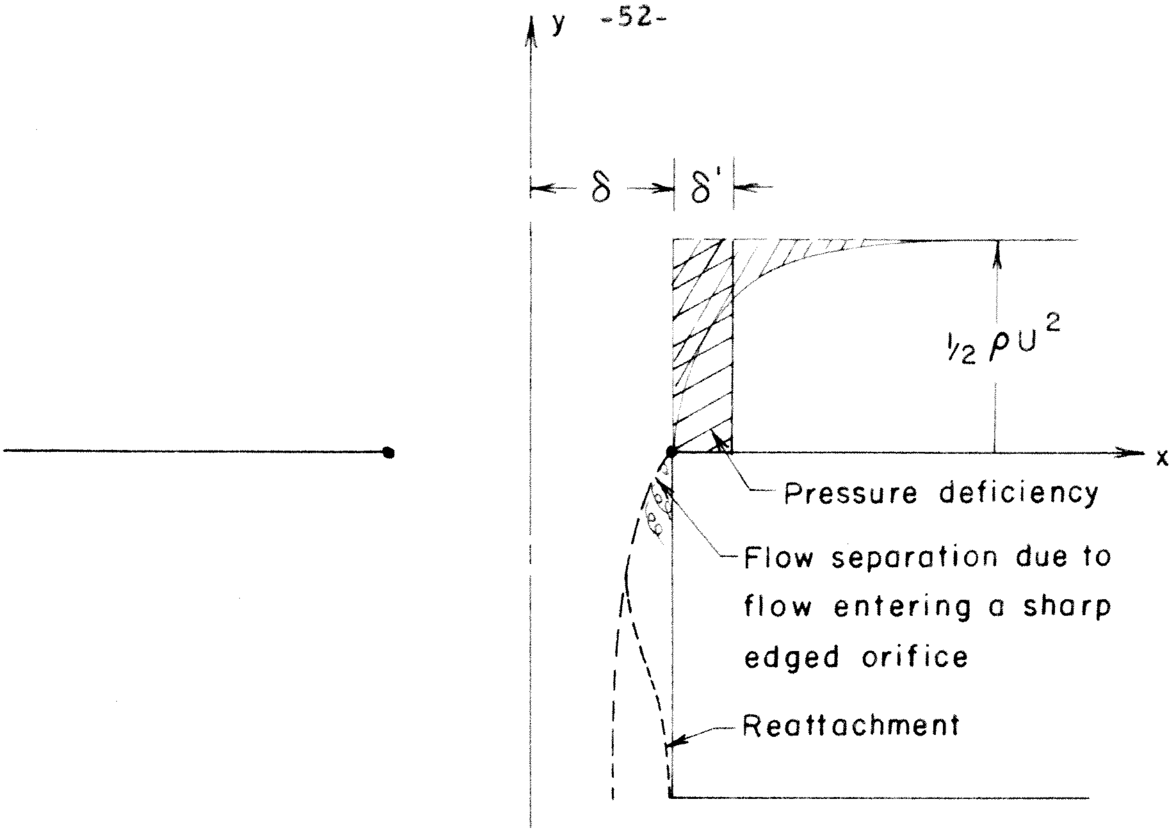

FIG. 23 - PRESSURE DEFICIENCY FROM FLOW INTO A SLOT

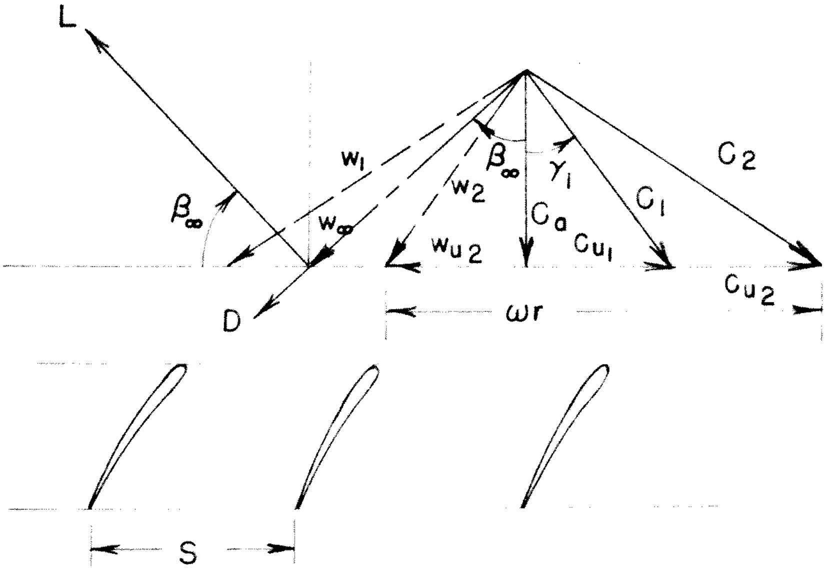

FIG. 24 - VELOCITY DIAGRAM SHOWING FLOW ENTERING AND LEAVING THE ROTOR WITH RELATIONS TO LIFT AND DRAG

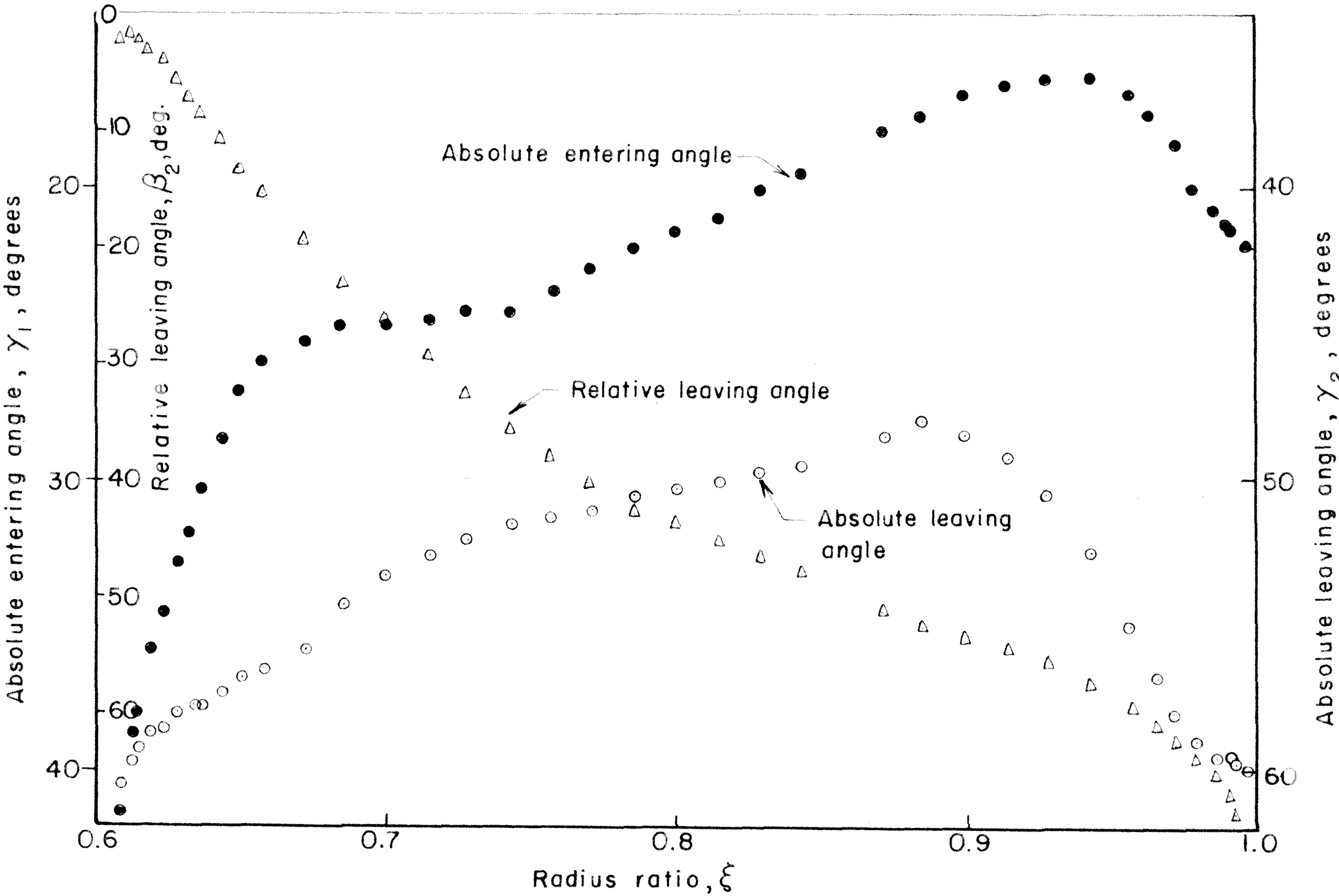

FIG. 25-FLOW ENTERING AND LEAVING ANGLES AS A FUNCTION OF RADIUS $\bar{\phi} = 0.348$, $\lambda = 0.0025$

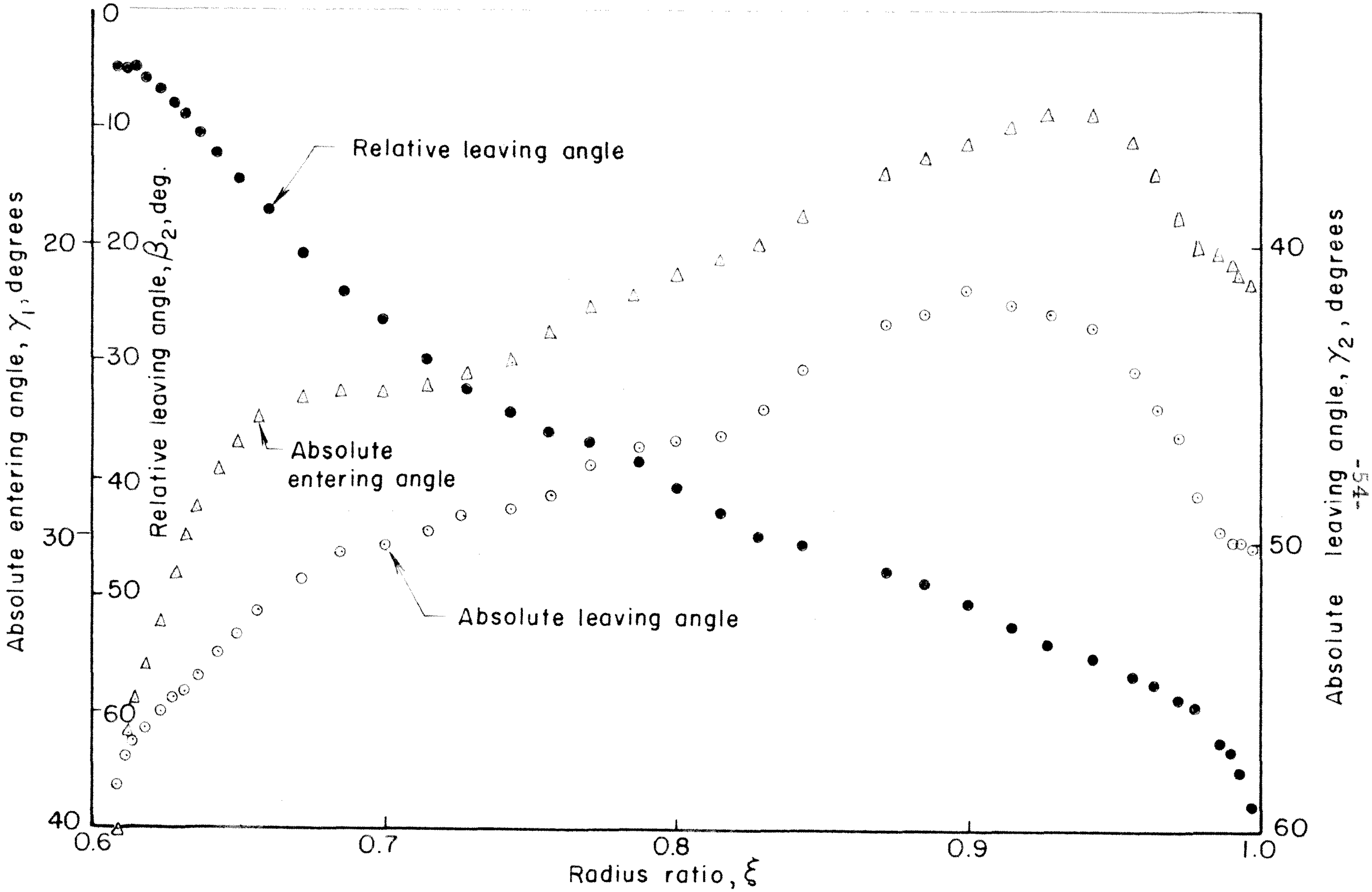

FIG. 26- FLOW ENTERING AND LEAVING ANGLES AS A FUNCTION OF RADIUS, $\bar{\phi} = 0.399$, $\lambda = 0.0025$

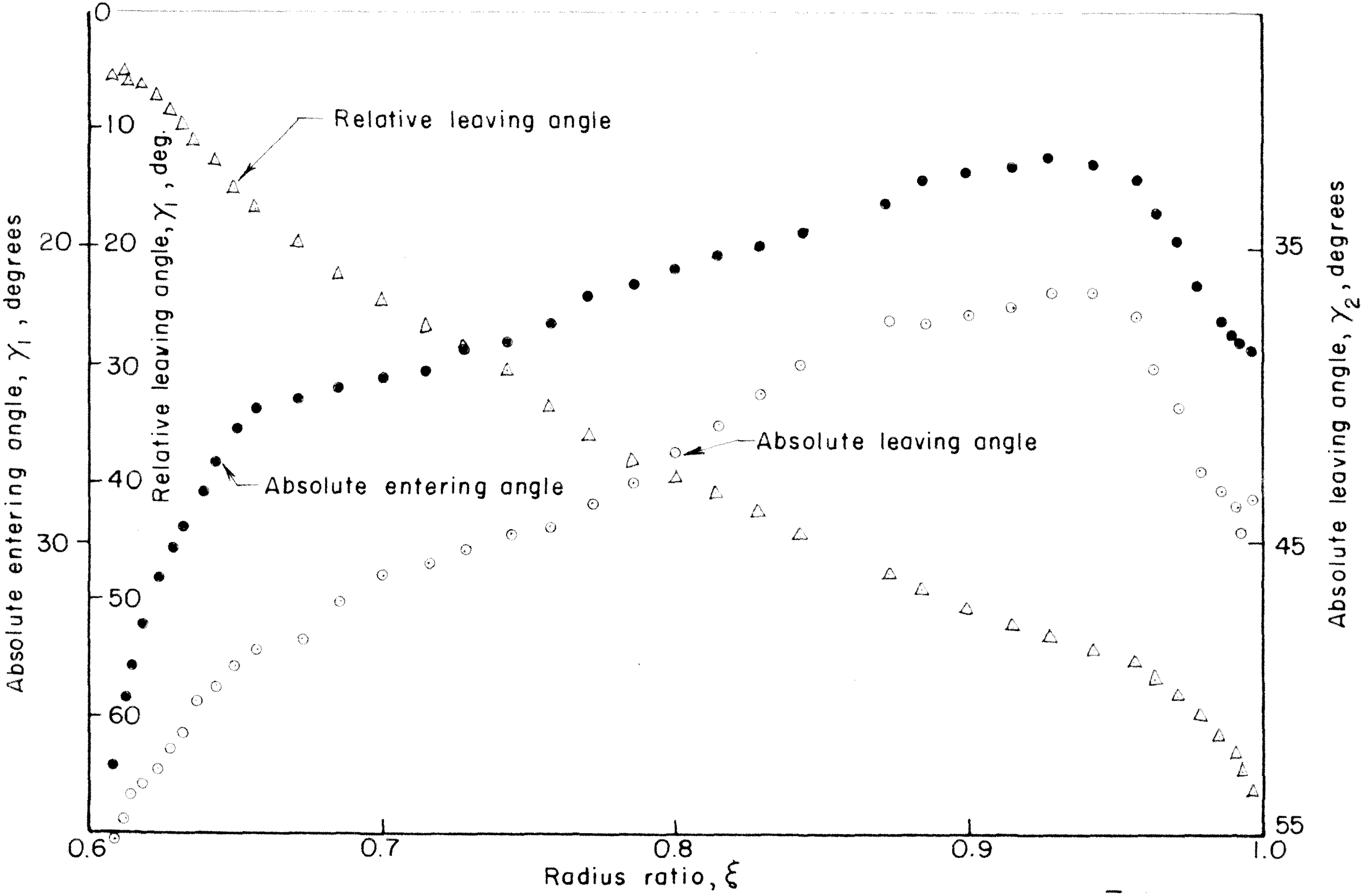

FIG. 27 — FLOW ENTERING AND LEAVING ANGLES AS FUNCTION OF RADIUS, $\bar{\phi}$ =0.443, λ=0.0025

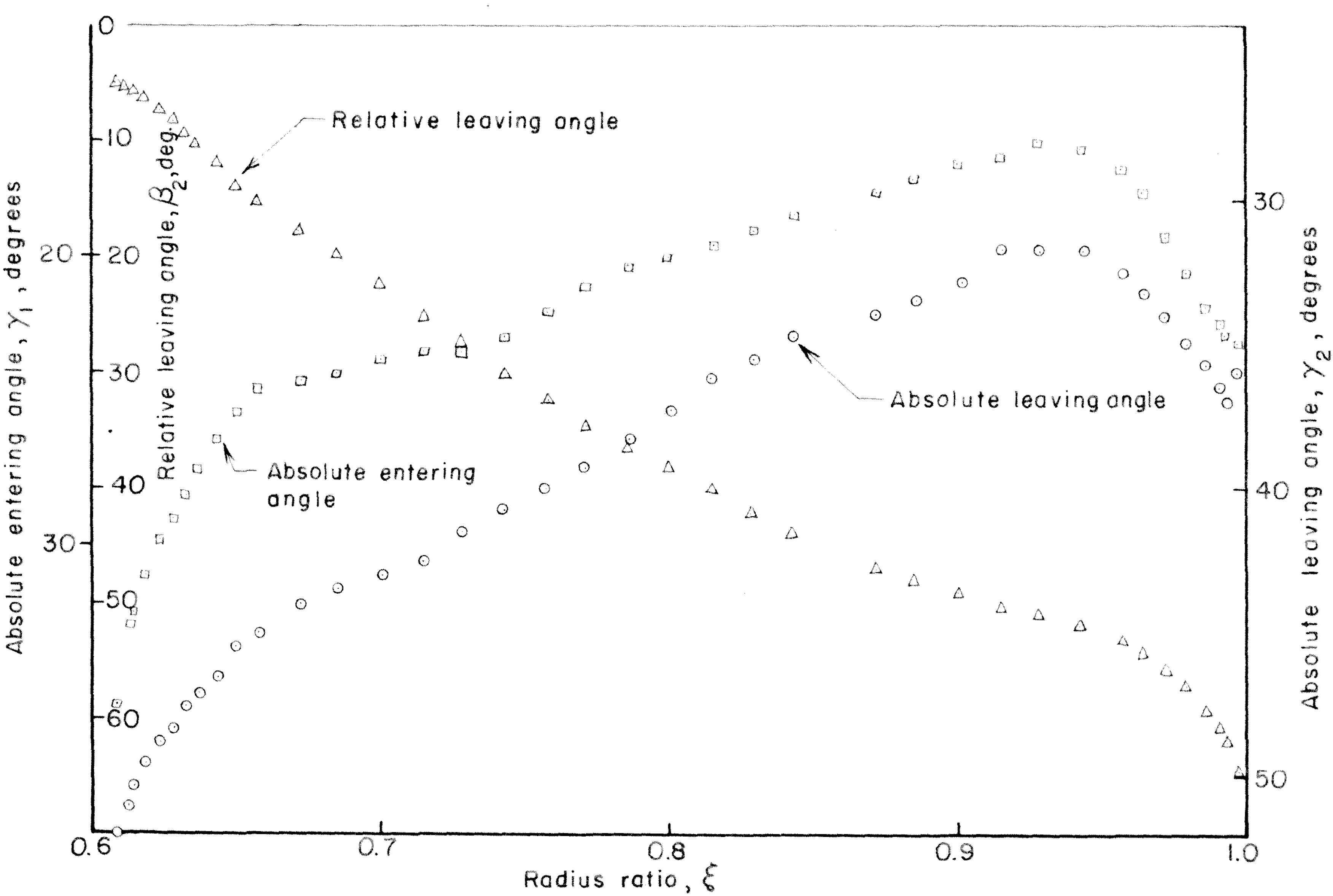

FIG. 28–FLOW ENTERING AND LEAVING ANGLE AS A FUNCTION OF RADIUS, $\bar{\phi} = 0.498$, $\lambda = 0.0025$

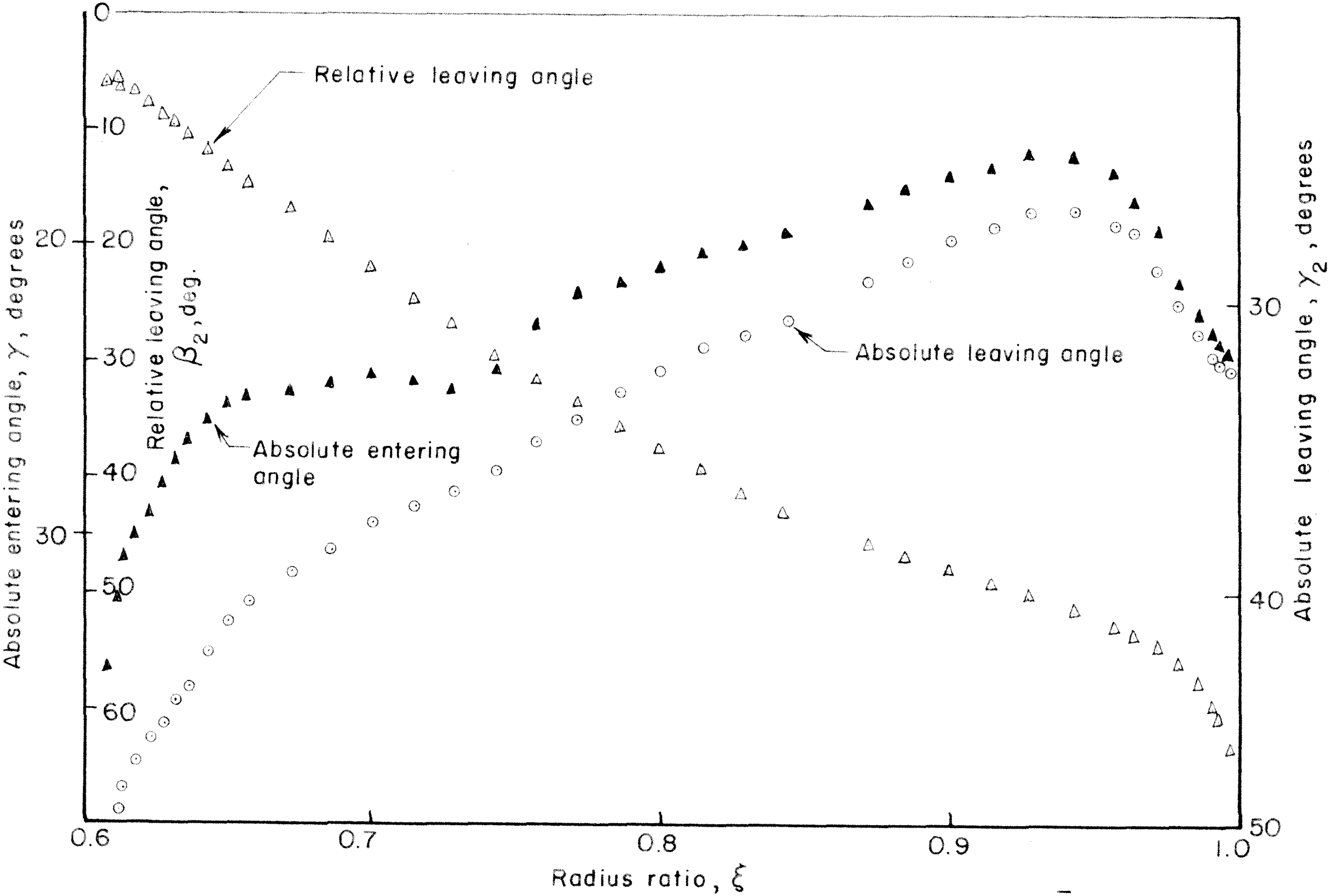

FIG. 29 – FLOW ENTERING AND LEAVING ANGLES AS A FUNCTION OF RADIUS, $\bar{\phi} = 0.548$, $\lambda = 0.0025$

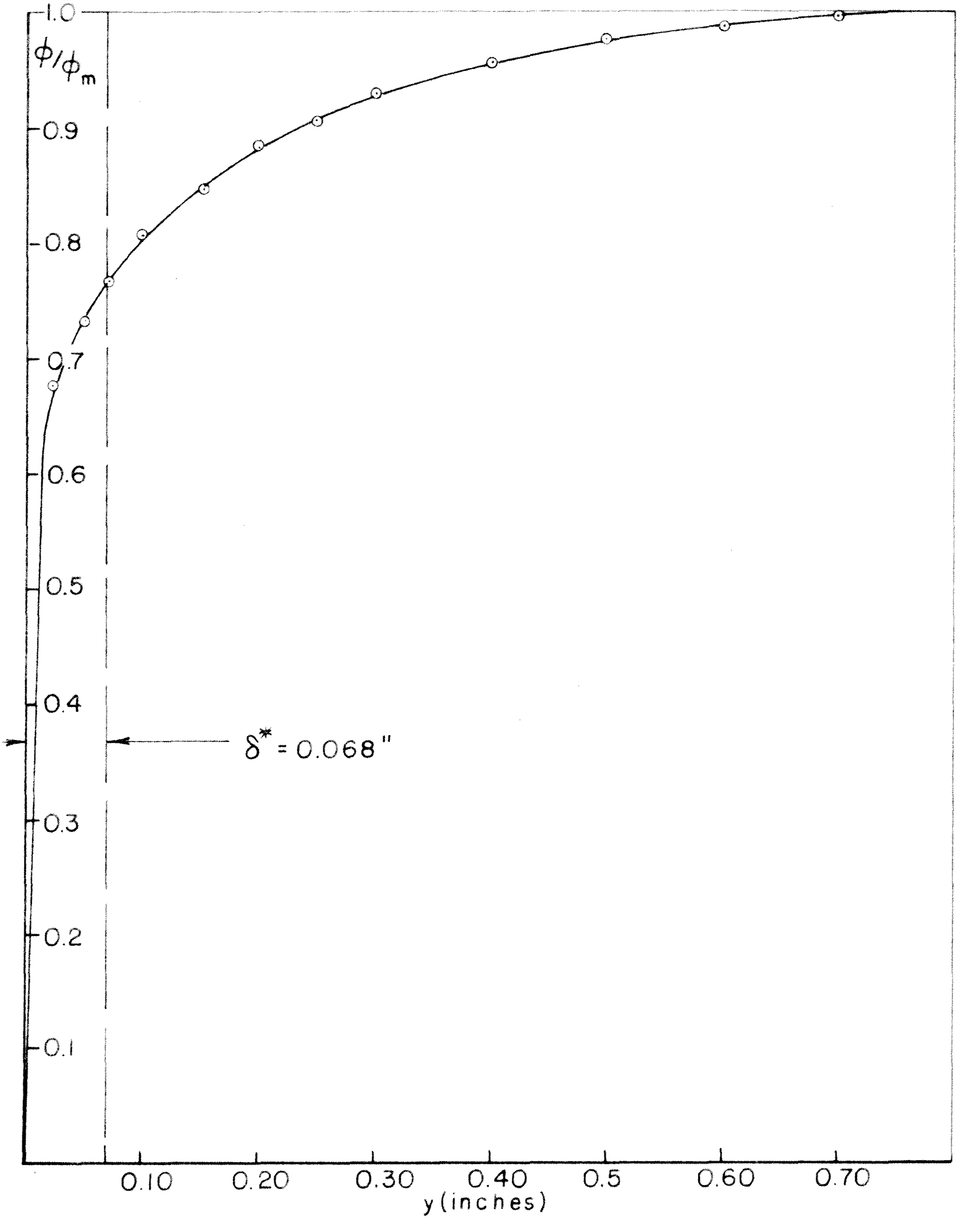

FIG. 30 - GRAPHICAL DETERMINATION OF BOUNDARY LAYER DISPLACEMENT THICKNESS δ^*

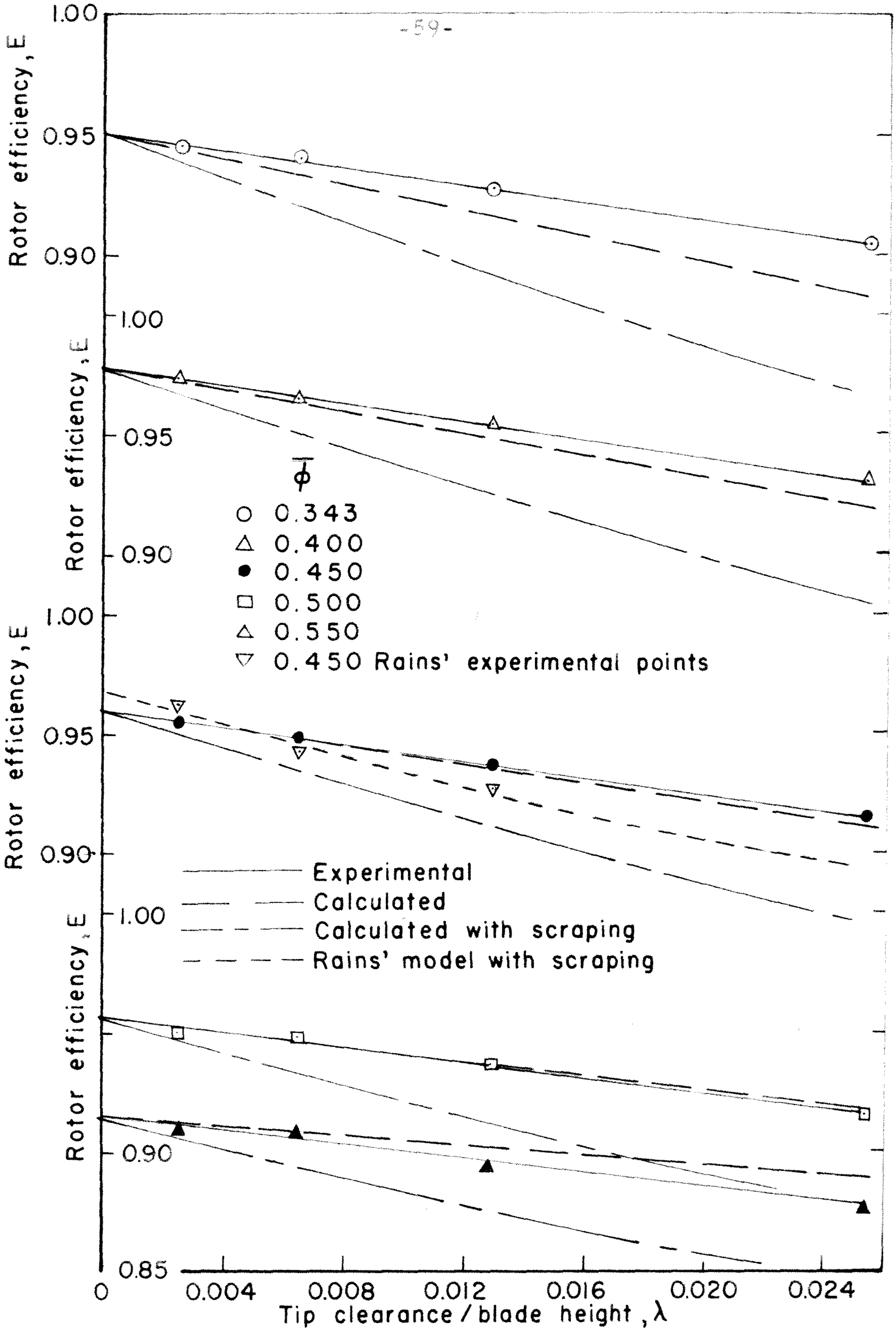

FIG. 31 COMPARISON OF CALCULATED AND EXPERIMENTAL ROTOR EFFICIENCY AS A FUNCTION OF TIP CLEARANCE FOR VARIOUS FLOW RATES